Journal of Computational Physics 238 (2013) 255–280

Contents lists available at SciVerse ScienceDirect

Journal of Computational Physics

journal homepage: www.elsevier.com/locate/jcp

Positivity-preserving DG and central DG methods for ideal MHD equations ☆

Yue Cheng [a,1], Fengyan Li [b,*], Jianxian Qiu [c], Liwei Xu [b,d]

[a] Department of Mathematics, Nanjing University, Nanjing, Jiangsu 210093, PR China
[b] Department of Mathematical Sciences, Rensselaer Polytechnic Institute, Troy, NY 12180, USA
[c] School of Mathematical Sciences, Xiamen University, Xiamen, Fujian 361005, PR China
[d] College of Mathematics and Statistics, Chongqing University, Chongqing 401331, PR China

ARTICLE INFO

Article history:
Received 15 May 2012
Received in revised form 26 October 2012
Accepted 20 December 2012
Available online 7 January 2013

Keywords:
MHD equations
Discontinuous Galerkin method
Central discontinuous Galerkin method
Positivity-preserving
High order accuracy

ABSTRACT

Ideal MHD equations arise in many applications such as astrophysical plasmas and space physics, and they consist of a system of nonlinear hyperbolic conservation laws. The exact density ρ and pressure p should be non-negative. Numerically, such positivity property is not always satisfied by approximated solutions. One can encounter this when simulating problems with low density, high Mach number, or much large magnetic energy compared with internal energy. When this occurs, numerical instability may develop and the simulation can break down. In this paper, we propose positivity-preserving discontinuous Galerkin and central discontinuous Galerkin methods for solving ideal MHD equations by following [X. Zhang, C.-W. Shu, Journal of Computational Physics 229 (2010) 8918–8934]. In one dimension, the positivity-preserving property is established for both methods under a reasonable assumption. The performance of the proposed methods, in terms of accuracy, stability and positivity-preserving property, is demonstrated through a set of one and two dimensional numerical experiments. The proposed methods formally can be of any order of accuracy.

1. Introduction

In this paper, we continue our investigation in developing highly accurate and robust numerical methods for ideal MHD equations [13–15,25]. This system models many important problems in a wide range of applications such as astrophysical plasmas and space physics, and it consists of a set of nonlinear hyperbolic conservation laws,

$$\frac{\partial \rho}{\partial t} + \nabla \cdot (\rho \mathbf{u}) = 0, \tag{1.1a}$$

$$\frac{\partial (\rho \mathbf{u})}{\partial t} + \nabla \cdot \left[\rho \mathbf{u}\mathbf{u}^{\mathrm{T}} + \left(p + \frac{1}{2}|\mathbf{B}|^2 \right) \mathbf{I} - \mathbf{B}\mathbf{B}^{\mathrm{T}} \right] = 0, \tag{1.1b}$$

$$\frac{\partial \mathbf{B}}{\partial t} + \nabla \cdot (\mathbf{u}\mathbf{B}^{\mathrm{T}} - \mathbf{B}\mathbf{u}^{\mathrm{T}}) = 0, \tag{1.1c}$$

☆ This research is partially supported by NSF DMS-0652481, NSF DMS-0636358 (RTG), NSF CAREER award DMS-0847241, NSF of China Grant No. 10931004 and ISTCP of China Grant No. 2010DFR00700, and an Alfred P. Sloan Research Fellowship.

* Corresponding author.
E-mail addresses: chengyue127@gmail.com (Y. Cheng), lif@rpi.edu (F. Li), jxqiu@xmu.edu.cn (J. Qiu), xul3@rpi.edu (L. Xu).
[1] Present address: Baidu, Inc. Baidu Campus, No. 10, Shangdi 10th Street, Haidian District, Beijing 100085, PR China.

0021-9991/$ - see front matter © 2013 Elsevier Inc. All rights reserved.
http://dx.doi.org/10.1016/j.jcp.2012.12.019

$$\frac{\partial E}{\partial t}+\nabla\cdot\left[\left(E+p+\frac{1}{2}|\mathbf{B}|^2\right)\mathbf{u}-\mathbf{B}(\mathbf{u}\cdot\mathbf{B})\right]=0, \tag{1.1d}$$

with an additional divergence-free constraint

$$\nabla\cdot\mathbf{B}=0. \tag{1.2}$$

Here ρ is the density, p is the hydrodynamic pressure, $\mathbf{u}=(u_x,u_y,u_z)^{\mathrm{T}}$ is the velocity field, and $\mathbf{B}=(B_x,B_y,B_z)^{\mathrm{T}}$ is the magnetic field. The total energy E is given by $E=\frac{1}{2}\rho|\mathbf{u}|^2+\frac{1}{2}|\mathbf{B}|^2+\frac{p}{\gamma-1}$ with γ as the ratio of the specific heats. We use the superscript T to denote the vector transpose. In addition, $\mathbf{I}$ is the identity matrix, $\nabla\cdot$ is the divergence operator, we further denote the momentum $\rho\mathbf{u}$ as $\mathbf{m}=(m_x,m_y,m_z)^{\mathrm{T}}$. Eqs. (1.1a), (1.1b), and (1.1d) are from the conservation of mass, momentum, and energy, and (1.1c) is the magnetic induction system. With compatible initial and boundary conditions, the divergence-free constraint (1.2) can be derived from the magnetic induction equations.

Besides the standard difficulty in simulating nonlinear hyperbolic equations, robust numerical algorithms for ideal MHD equations often require the divergence-free constraint in (1.2) being properly imposed [7,10,21,3]. In [13–15,25], we proposed and investigated strategies to obtain locally or globally divergence-free approximations for the magnetic field in discontinuous Galerkin (DG) and central DG framework. Besides the designed high order accuracy, these divergence-free methods demonstrate much improved numerical stability than the base methods without any divergence-free treatment. On the other hand, in the simulation of some examples including certain cloud–shock interaction problems, it is observed that the appearance of negative pressure can also lead to numerical instability, and such instability may not be removed by simply working with divergence-free schemes. In fact both density ρ and pressure p in exact solutions should be non-negative. Numerically, such positivity property is not always satisfied by approximated solutions, and this may cause the loss of hyperbolicity of the system and lead to instability of the simulation. For instance, one can encounter this when simulating problems with low density, high Mach number, or much large magnetic energy compared with internal energy. In this paper, we are interested in developing high order DG and central DG methods for (1.1), (1.2) which preserve positivity of both density and pressure. More specifically, we propose positivity-preserving limiters with which the cell average of the DG or central DG solution has positive density and pressure at discrete time t_n as long as they are initially positive. It is in general difficult to design positivity-preserving schemes which also satisfy the divergence-free constraint exactly. In this paper, the positivity-preserving limiters are presented for standard DG and central DG methods defined in Sections 3.1 and 3.2 where the divergence constraint is not considered. We want to point out that by utilizing the intrinsic local nature of both methods, one can also apply locally divergence-free approximations [13] straightforwardly in the present framework without affecting the positivity-preserving property of the overall algorithm (see also Remark 3.1).

In the context of ideal MHD equations, a positivity-preserving limiter was designed and analyzed in [22] for a second order finite volume method. The resulting scheme is conservative in one dimension, and it is nonconservative in higher dimensions with a source term added to the magnetic induction equation and properly discretized in order to take into account the normal jump in the magnetic field. Such modified magnetic induction equation allowing magnetic monopoles was also used in [12] for a positive scheme combining both HLL and Roe methods. In [5], a hybrid strategy was proposed for the positivity of pressure. It involves a linearized Riemann solver working directly with the entropy density equation instead of the total energy Eq. (1.1d) in the absence of magnetosonic shocks, and a standard Riemann solver based on (1.1) elsewhere. The overall strategy relies on switches to indicate where each Riemann solver should be applied.

On the other hand, for compressible Euler equations (which are the same as ideal MHD equations when the magnetic field is zero), an innovative positivity-preserving technique was recently introduced and analyzed by Zhang and Shu in [27] for finite volume methods and DG methods with arbitrary order of accuracy. This technique can be regarded as generalization of the maximum-principle-satisfying limiters for scalar conservation laws [26] and the positivity-preserving schemes for compressible Euler equations in [17]. It starts with a first order positivity-preserving scheme as a building block, followed by a necessary condition to ensure the positivity-preserving property of the methods of higher order accuracy. A simple local limiter is then designed and analyzed to enforce the sufficient condition without destroying the accuracy and conservation of the schemes. The limiter was first presented when the time discretization is forward Euler method, then high order accuracy in time is achieved with the use of strong stability preserving (SSP) time discretizations which can be written as a convex combination of forward Euler methods. In the present work, we apply the positivity-preserving technique of Zhang and Shu to DG methods in solving ideal MHD system, and we also propose such technique to central DG methods. In one dimension, the positivity-preserving property of both the DG and central DG methods is established theoretically under a reasonable assumption. In higher than one dimension, the numerically relevant Riemann problem allows nonzero divergence in the magnetic field, therefore the numerical divergence often needs to be taken into account in devising positivity-preserving schemes, see [22]. We here formally extend the proposed positivity-preserving limiters to two dimensions as in [27]. Though without rigorous analysis, the performance of the methods in terms of accuracy, stability, and being positivity-preserving, are successfully demonstrated through a set of one and two dimensional numerical experiments. Both DG and central DG methods use piecewise smooth functions as approximations, and they have proved themselves to be a good candidate to accurately and reliably simulate many linear and nonlinear problems including nonlinear conservations laws [8,16]. Compared with DG methods, central DG methods evolve two copies of numerical solutions and do not use any numerical flux (which is an approximate Riemann solver). This implies that one cannot rely on properly designed numerical Riemann

solvers as in [5,22] to devise positivity-preserving central DG methods. In fact, the present work is the first to examine the positivity preserving property in the central DG framework (see also the concluding remarks in Section 5). Even with the difference between DG and central DG methods, one will see that the positivity-preserving limiters for both methods turn out to be very similar. The methods are presented for one dimension and two dimensions on Cartesian meshes in this paper, but there is no essential difficulty to extend them to three dimensions and triangular meshes [23].

For ideal MHD equations, part of the techniques developed by Zhang and Shu [27] was recently used in [1] to design self-adjusting positivity-preserving high order finite volume WENO (weighted essentially non-oscillatory) schemes, with the ADER time discretization [2] in the numerical experiments. Such time discretizations are different from SSP time discretizations, whose structure of being a convex combination of the first order Euler methods is an important component for the methods in [27] (and the one-dimensional schemes in this paper) to achieve *provable* positivity-preserving property with high order accuracy. To thoroughly understand the methods in [1], analysis different from the one in [27] would be needed. In [24], a similar scaling procedure as in [27] was used to remove the negative pressure in numerically simulating the double Mach reflection problem in compressible Euler equations using DG methods.

The remainder of the paper is organized as follows. Section 2 is devoted to one dimension. Here we establish the positivity-preserving property of the first order DG method with the Lax–Friedrichs flux and the first order central DG method. With these building blocks, necessary conditions are given to obtain positivity-preserving higher order DG and central DG methods. Such conditions can be achieved through some positivity-preserving limiters. These methods are formally extended to two dimensions in Section 3 on Cartesian meshes. In Section 4, numerical experiments are carried out to demonstrate the accuracy, stability, and positivity-preserving properties of the methods in one and two dimensions. Concluding remarks are made in Section 5.

2. One-dimensional case

In this section, we will propose and analyze positivity-preserving DG and central DG methods for one-dimensional ideal MHD systems. For DG methods, the positivity-preserving technique is a direct generalization of the one in [27] for compressible Euler equations which can be regarded as a special case of the ideal MHD system (1.1) with a zero magnetic field.

With $\mathbf{U} = (\rho, \mathbf{m}^T, \mathbf{B}^T, E)^{\mathrm{T}}$, one-dimensional ideal MHD system can be written as

$$\frac{\partial \mathbf{U}}{\partial t} + \frac{\partial}{\partial x}\mathbf{F}(\mathbf{U}) = \mathbf{0}, \tag{2.3}$$

where

$$\mathbf{F}(\mathbf{U}) = \left(m_x, \frac{m_x^2}{\rho} + p + \frac{1}{2}|\mathbf{B}|^2, \frac{m_x m_y}{\rho} - B_x B_y, \frac{m_x m_z}{\rho} - B_x B_z, 0, \frac{m_x B_y - m_y B_x}{\rho}, \frac{m_x B_z - m_z B_x}{\rho}, \frac{1}{\rho}(m_x(E + p + \frac{1}{2}|\mathbf{B}|^2) - B_x \mathbf{m}\cdot\mathbf{B})\right)^{\mathrm{T}}.$$

We define an admissible set G,

$$G = \{\mathbf{U}: \ \rho > 0 \text{ and } p(\mathbf{U}) > 0\}, \tag{2.4}$$

with $p(\mathbf{U}) = (\gamma - 1)(E - \frac{1}{2}\frac{|\mathbf{m}|^2}{\rho} - \frac{1}{2}|\mathbf{B}|^2)$. One can verify that G is a convex set since $p(\mathbf{U})$ is a concave function of $\mathbf{U}$ when $\rho > 0$. In one dimension, the divergence-free condition $\nabla \cdot \mathbf{B} = 0$ in (1.2) is reduced to $B_x =$ constant. In this section, we assume $B_x = B_{0x}$ at $t = 0$, with B_{0x} being a given constant. The relevant admissible set is $G = G_{B_{0x}} = \{\mathbf{U}: B_x = B_{0x}, \ \rho > 0 \text{ and } p(\mathbf{U}) > 0\}$. That is, the B_x component of all admissible states in G takes the same value B_{0x}. Throughout this section, G always means $G_{B_{0x}}$. In addition, we make the following assumption.

Assumption $\mathcal{P}$. Consider the following one-dimensional Riemann problem for the ideal MHD system

$$\begin{cases} \frac{\partial \mathbf{U}}{\partial t} + \frac{\partial}{\partial x}\mathbf{F}(\mathbf{U}) = \mathbf{0}, \\ \mathbf{U}(x,0) = \begin{cases} \mathbf{U}_l, & x < 0, \\ \mathbf{U}_r, & x > 0. \end{cases} \end{cases} \tag{2.5}$$

where $B_x = B_{0x}$ at $t = 0$. We assume that $\mathbf{U}_l, \mathbf{U}_r$ belonging to G implies that the exact solution $\mathbf{U}(x,t) \in G$.

It is reasonable to make above assumption in order to design a positivity-preserving numerical method for the ideal MHD system. We will not consider the more subtle case when vacuum (with $\rho = 0$) may develop [20].

2.1. Positivity-preserving DG schemes

To define DG methods, we start with a mesh $\{I_i\}_i$ of the computational domain $\Omega = (x_{min}, x_{max})$, with $I_i = (x_i, x_{i+1})$. Without loss of generality, the mesh is assumed to be uniform with a meshsize Δx. We further introduce a finite dimensional discrete space

$$\mathcal{U}_h = \{\mathbf{u} = (u_1, \ldots, u_8)^{\mathrm{T}} : u_l|_{I_i} \in P^k(I_i), \forall l, i\},$$

where $P^k(I_i)$ consists of polynomials in I_i of degree at most k. Note that any function $\mathbf{u}$ in $\mathcal{U}_h$ is piecewise defined, and it is discontinuous at grid points. We use $\mathbf{u}_i^-$ and $\mathbf{u}_i^+$ to denote the limit of $\mathbf{u}$ from the left and the right of x_i, respectively, $\forall i$. A standard semi-discrete DG method for (2.3) is given as follows: look for $\mathbf{U}_h \in \mathcal{U}_h$, such that $\forall \mathbf{u} \in \mathcal{U}_h$, and $\forall i$,

$$\int_{I_i} \frac{\partial \mathbf{U}_h}{\partial t} \cdot \mathbf{u}\, dx - \int_{I_i} \mathbf{F}(\mathbf{U}_h) \cdot \frac{\partial \mathbf{u}}{\partial x} dx + \mathbf{h}_{i+1}\mathbf{u}_{i+1}^- - \mathbf{h}_i \mathbf{u}_i^+ = 0. \tag{2.6}$$

The function $\mathbf{h} = \mathbf{h}(\mathbf{U}_h^-, \mathbf{U}_h^+)$ is a single-valued numerical flux which is consistent to $\mathbf{F}$, namely $\mathbf{h}(\mathbf{U}, \mathbf{U}) = \mathbf{F}(\mathbf{U})$. Such DG methods, like many other numerical methods, usually are not positivity-preserving. We want to propose a positivity-preserving limiter, such that when it is applied to DG methods with a properly chosen numerical flux, the cell average of the DG solution $\bar{\mathbf{U}}_h$ will belong to the admissible set G at each discrete time t_n.

By following [27], to design positivity-preserving limiters for DG methods of arbitrary accuracy when explicit SSP time discretizations are used (these are the time discretizations we consider in this work, and they can be written as a convex combination of the first order forward Euler methods), one only needs to find a first order positivity-preserving DG method with the forward Euler time discretization. For this, we start with $k = 0$, apply the first order forward Euler time discretization in (2.6), and get

$$\mathbf{U}_i^{n+1} = \mathbf{U}_i^n - \lambda\big(\mathbf{h}(\mathbf{U}_i^n, \mathbf{U}_{i+1}^n) - \mathbf{h}(\mathbf{U}_{i-1}^n, \mathbf{U}_i^n)\big). \tag{2.7}$$

Here $\lambda = \frac{\Delta t}{\Delta x}$, $\Delta t = t_{n+1} - t_n$ is the time step, and $\mathbf{U}_i^n$ approximates the cell average of the exact solution in I_i at time t_n. In actual simulations Δt often depends on n. The first order scheme (2.7) with its numerical flux $\mathbf{h}(\cdot,\cdot)$ is called positivity-preserving, if one can imply $\mathbf{U}_j^{n+1} \in G$ for all j as long as $\mathbf{U}_j^n \in G$ for all j. In next subsection, we will prove and numerically confirm that with a simple Lax–Friedrichs flux, namely,

$$\mathbf{h}(\mathbf{u}^-, \mathbf{u}^+) = \frac{1}{2}(\mathbf{F}(\mathbf{u}^-) + \mathbf{F}(\mathbf{u}^+) - a_x(\mathbf{u}^+ - \mathbf{u}^-)), \tag{2.8}$$

where

$$a_x = ||(|u_x| + c_f^x)(\cdot, t_n)||_\infty \tag{2.9}$$

and c_f^x is the fast speed of the system in x-direction [18], the first order DG method (2.7) is positivity-preserving under Assumption $\mathcal{P}$ and a reasonable CFL condition.

2.1.1. Positivity-preserving property of the first order Lax–Friedrichs DG method

Lemma 2.1. *Under Assumption $\mathcal{P}$, the first order DG method with the Lax–Friedrichs numerical flux defined in (2.7)–(2.9) is positivity-preserving under a CFL condition*

$$\lambda a_x \leqslant \alpha_0, \tag{2.10}$$

with $\alpha_0 = \frac{1}{2}$. That is, if $\mathbf{U}_i^n \in G, \forall i$, then $\mathbf{U}_i^{n+1} \in G, \forall i$. In addition, the numerical B_x stays as constant.

Proof. With the numerical flux in (2.8), the fifth component $\mathbf{U}_i^n$ does not change with respect to n, therefore the numerical B_x stays as a constant. The proof for the positivity-preserving property follows Appendix in [17] which is for the compressible Euler equation. We here provide more details of the analysis. Assume $\mathbf{U}_i^n \in G$, $\forall i$, we want to show that $\mathbf{U}_i^{n+1}$, computed from (2.7)–(2.9), is in G, $\forall i$.

Step 1. First we consider an auxiliary Riemann problem

$$\begin{cases} \frac{\partial \mathbf{V}}{\partial t} + \frac{\partial}{\partial x}(\mathbf{F}(\mathbf{V}) + a_x \mathbf{V}) = \mathbf{0}, \\ \mathbf{V}(x, t_\star) = \begin{cases} \mathbf{U}_{i-1}^n, & x < x_\star, \\ \mathbf{U}_i^n, & x > x_\star, \end{cases} \end{cases} \tag{2.11}$$

with its solution denoted as $\mathbf{V} = \mathbf{V}(x, t; x_\star, t_\star, \mathbf{U}_{i-1}^n, \mathbf{U}_i^n), t \geqslant t_\star$. Note that $\mathbf{U}(x,t) = \mathbf{V}(x + x_\star + a_x t, t + t_\star)$ satisfies the Riemann problem (2.5) with $\mathbf{U}_l = \mathbf{U}_{i-1}^n$ and $\mathbf{U}_r = \mathbf{U}_i^n$. Based on Assumption $\mathcal{P}, \mathbf{U}(\cdot, t) \in G$, and therefore $\mathbf{V}(\cdot, t; x_\star, t_\star, \mathbf{U}_{i-1}^n, \mathbf{U}_i^n) \in G, t \geqslant t_\star$. Similarly, if we replace a_x with $-a_x$ in (2.11), the solution to this new problem will also belong to G.

Step 2. Next we consider

$$\begin{cases} \frac{\partial \mathbf{U}}{\partial t} + \frac{\partial}{\partial x}(\mathbf{F}(\mathbf{U}) + a_x \mathbf{U}) = \mathbf{0}, \\ \mathbf{U}(x, t_n) = \mathbf{U}_i^n, \qquad \text{when } x \in I_i. \end{cases} \tag{2.12}$$

It is easy to see that the eigenvalues of the Jacobian of $\mathbf{F}(\mathbf{U}) + a_x \mathbf{U}$ are non-negative and no more than $2a_x$. Let $t_{n+1} = t_n + \Delta t$, with $\Delta t \leqslant \frac{\Delta x}{2a_x}$. In the time interval $[t_n, t_{n+1}]$, the solution to (2.12) consists of many Riemann problems, with each stemming

from $x = x_i$ at $t = t_n, \forall i$ (see Fig. 2.1). Moreover, these Riemann problems will not intersect each other and the exact solution $\mathbf{U}$ is given by $\mathbf{U}(x,t) = \mathbf{V}(x,t;x_i,t_n,\mathbf{U}_{i-1}^n,\mathbf{U}_i^n)$ for $x \in I_i = (x_i, x_{i+1})$ and $t \in [t_n, t_{n+1}]$, therefore $\mathbf{U}(x,t) \in G$ within this time interval. If we further integrate Eq. (2.12) over the control volume $I_i \times [t_n, t_{n+1}]$, then

$$\begin{aligned}\tilde{\mathbf{U}}_i &:= \frac{1}{\Delta x}\int_{I_i}\mathbf{U}(x,t_{n+1})dx = \frac{1}{\Delta x}\int_{I_i}\mathbf{U}(x,t_n)dx - \frac{1}{\Delta x}\left(\int_{t_n}^{t_{n+1}}(\mathbf{F}(\mathbf{U}) + a_x\mathbf{U})(x_{i+1},t) - (\mathbf{F}(\mathbf{U}) + a_x\mathbf{U})(x_i,t)dt\right)\\ &= \mathbf{U}_i^n - \lambda\big(\mathbf{F}(\mathbf{U}_i^n) + a_x\mathbf{U}_i^n - \mathbf{F}(\mathbf{U}_{i-1}^n) - a_x\mathbf{U}_{i-1}^n\big).\end{aligned} \tag{2.13}$$

Since G is a convex set, $\mathbf{U}(x,t_{n+1}) \in G$ implies $\tilde{\mathbf{U}}_i = \frac{1}{\Delta x}\int_{I_i}\mathbf{U}(x,t_{n+1})dx \in G$. For the last equality (2.13), we use $\mathbf{U}(x_i,t) = \mathbf{U}_{i-1}^n,\ \forall i$ for $t \in (t_n, t_{n+1})$ and this is due to the self-similarity property of the solution to the Riemann problem. Similarly, if we replace a_x with $-a_x$ in (2.12), and consider

$$\begin{cases}\frac{\partial \mathbf{U}}{\partial t} + \frac{\partial}{\partial x}(\mathbf{F}(\mathbf{U}) - a_x\mathbf{U}) = \mathbf{0},\\ \mathbf{U}(x,t_n) = \mathbf{U}_i^n, \qquad\qquad \text{when } x \in I_i,\end{cases} \tag{2.14}$$

then $\tilde{\tilde{\mathbf{U}}}_i \in G$, with

$$\tilde{\tilde{\mathbf{U}}}_i := \mathbf{U}_i^n - \lambda\big(\mathbf{F}(\mathbf{U}_{i+1}^n) - a_x\mathbf{U}_{i+1}^n - \mathbf{F}(\mathbf{U}_i^n) + a_x\mathbf{U}_i^n\big). \tag{2.15}$$

Step 3. Note that $\mathbf{U}_i^{n+1} = \frac{\tilde{\mathbf{U}}_i + \tilde{\tilde{\mathbf{U}}}_i}{2}, \forall i$ indeed is the solution at $t = t_{n+1}$ to the first order DG method with the Lax–Friedrichs numerical flux defined in (2.7)–(2.9). With the convexity of the set G, we now conclude that $\mathbf{U}_i^{n+1} \in G$. □

Remark 2.2. In Lemma 2.1, the upper bound for the CFL condition is $\alpha_0 = 1/2$. This is the same as that for the compressible Euler equation in [17], and it ensures the local Riemann problems considered in the proof of Lemma 2.1 (see Step 2) will not intersect each other. The result in [17] is further improved in [27] with $\alpha_0 = 1$ through a purely algebraic proof by showing $\mathbf{U}_{i-1}^n + \frac{1}{a_x}\mathbf{F}(\mathbf{U}_{i-1}^n)$ and $\mathbf{U}_{i+1}^n - \frac{1}{a_x}\mathbf{F}(\mathbf{U}_{i+1}^n)$ belong to G. Unfortunately such improvement can not be made for the ideal MHD system as numerical tests show that $\mathbf{U}_{i-1}^n + \frac{1}{a_x}\mathbf{F}(\mathbf{U}_{i-1}^n)$ and $\mathbf{U}_{i+1}^n - \frac{1}{a_x}\mathbf{F}(\mathbf{U}_{i+1}^n)$ may not be in G. This is also implied by the numerical experiments reported in Table 2.2. On the other hand, α_0 larger than 1/2 can be used in actual simulations.

As the core result for developing high order positivity-preserving DG methods, Lemma 2.1 relies on Assumption $\mathcal{P}$. Next we will present a set of numerical experiments to validate this lemma. We start with three vectors $\mathbf{U}_{i-1}^n, \mathbf{U}_i^n$ and $\mathbf{U}_{i+1}^n$ which take random values. In particular u_x, u_y, u_z, B_y and B_z are from $U(-\gamma_1,\gamma_1)$, ρ is from $U(0,\gamma_2)$, and p is from $U(0,\gamma_3)$. The constant component B_x is from $U(-\gamma_4,\gamma_4)$. Here $U(\gamma_\star,\gamma_{\star\star})$ is the uniform distribution on $(\gamma_\star,\gamma_{\star\star})$. We also vary the CFL number λa_x within $[1/2, 1]$. For each set of parameters γ_i, $i = 1,\ldots 4$ and λa_x, we conduct 10^5 random experiments, compute $\mathbf{U}_i^{n+1}$ from (2.7)–(2.9), and count the total number of occurrence of negative pressure, namely when $p(\mathbf{U}_i^{n+1}) < 0$. The results in Table 2.1 are collected when $\lambda a_x = 1/2$, and they confirm that the first order Lax–Friedrichs DG method (2.7)–(2.9) is positivity-preserving under the CFL condition 2.10 with $\lambda a_x = (\leqslant)\alpha_0 = 1/2$. Numerical tests further indicate that this positivity-preserving property holds for a larger CFL condition with $\alpha_0 = 9/10$ (the numerical results are not included), yet not always for $\alpha_0 = 1$ as in [27] for the compressible Euler equations. This is illustrated by the results in Table 2.2 with $\lambda a_x = 1$. On the other hand, when $\lambda a_x = 1$ negative pressure occurs very rarely (in less than 0.01% of all the experiments we have carried out), and this partially explains the satisfactory performance of the positivity-preserving high order DG methods when $\lambda a_x = 1$ is used in MHD simulations (see Section 4).

2.1.2. Positivity-preserving DG methods with higher order accuracy

Once a first order positivity-preserving DG method (2.7) is identified with the first order forward Euler time discretization, one can proceed exactly as in [27] to consider DG methods with general order of accuracy. Since SSP time discretizations are used in this work, we only need to consider the scheme satisfied by the cell average of the DG solution with the forward Euler time discretization, given as

$$\bar{\mathbf{U}}_i^{n+1} = \bar{\mathbf{U}}_i^n - \lambda(\mathbf{h}(\mathbf{U}_{i+1}^{n,-},\mathbf{U}_{i+1}^{n,+}) - \mathbf{h}(\mathbf{U}_i^{n,-},\mathbf{U}_i^{n,+})). \tag{2.16}$$

Here $\bar{\mathbf{U}}_i^n$ is the cell average of the DG solution $\mathbf{U}_h$ on I_i at time t_n. We also use $\mathbf{U}_i^n = \mathbf{U}(x_i,t_n)$.

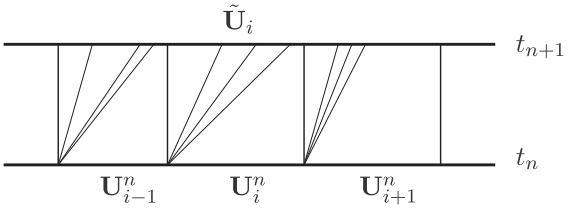

Fig. 2.1. Illustration for the problem defined in (2.12).

Table 2.1
To verify the positivity-preserving property of the first order Lax–Friedrichs DG method (2.7)–(2.9). u_x, u_y, u_z, B_y, B_z is from $U(-\gamma_1, \gamma_1)$, ρ is from $U(0, \gamma_2)$, p is from $U(0, \gamma_3)$, and B_x is from $U(-\gamma_4, \gamma_4)$. † = the total number of occurrence of negative pressure in 10^5 random experiments. The CFL condition is $\lambda a_x = \alpha_0 = 1/2$. B_x is continuous.

α_0	γ_1	γ_2	γ_3	γ_4	†	α_0	γ_1	γ_2	γ_3	γ_4	†
1/2	10	10^{-4}	10^{-4}	1	0	1/2	10	100	1	10	0
1/2	10	10^{-4}	10^{-4}	10	0	1/2	10	100	1	100	0
1/2	10	10^{-4}	10^{-4}	100	0	1/2	100	10^{-4}	10^{-4}	1	0
1/2	10	10^{-4}	1	1	0	1/2	100	10^{-4}	10^{-4}	10	0
1/2	10	10^{-4}	1	10	0	1/2	100	10^{-4}	10^{-4}	100	0
1/2	10	10^{-4}	1	100	0	1/2	100	10^{-4}	1	1	0
1/2	10	1	10^{-4}	1	0	1/2	100	10^{-4}	1	10	0
1/2	10	1	10^{-4}	10	0	1/2	100	10^{-4}	1	100	0
1/2	10	1	10^{-4}	100	0	1/2	100	1	10^{-4}	1	0
1/2	10	1	1	1	0	1/2	100	1	10^{-4}	10	0
1/2	10	1	1	10	0	1/2	100	1	10^{-4}	100	0
1/2	10	1	1	100	0	1/2	100	1	10^{-4}	1000	0
1/2	10	10	10^{-4}	1	0	1/2	100	1	10^{-4}	10000	0
1/2	10	10	10^{-4}	10	0	1/2	100	1	10^{-4}	10000	0
1/2	10	10	10^{-4}	100	0	1/2	100	1	1	1	0
1/2	10	100	10^{-4}	100	0	1/2	100	1	1	10	0
1/2	10	100	1	1	0	1/2	100	1	1	100	0

Table 2.2
To verify the positivity-preserving property of the first order Lax–Friedrichs DG method (2.7)–(2.9). u_x, u_y, u_z, B_y, B_z is from $U(-\gamma_1, \gamma_1)$, ρ is from $U(0, \gamma_2)$, p is from $U(0, \gamma_3)$, and B_x is from $U(-\gamma_4, \gamma_4)$. † = the total number of occurrence of negative pressure in 10^5 random experiments. *The CFL condition is* $\lambda a_x = \alpha_0 = 1$. B_x *is continuous.*

α_0	γ_1	γ_2	γ_3	γ_4	†	α_0	γ_1	γ_2	γ_3	γ_4	†
1	10	10^{-4}	10^{-4}	1	0	1	100	10^{-4}	10^{-4}	1	0
1	10	10^{-4}	10^{-4}	10	0	1	100	10^{-4}	10^{-4}	10	0
1	10	10^{-4}	10^{-4}	100	0	1	100	10^{-4}	10^{-4}	100	0
1	10	10^{-4}	1	1	0	1	100	10^{-4}	1	1	0
1	10	10^{-4}	1	10	0	1	100	10^{-4}	1	10	0
1	10	10^{-4}	1	100	0	1	100	10^{-4}	1	100	0
1	10	1	10^{-4}	1	0	1	100	1	10^{-4}	1	0
1	10	1	10^{-4}	10	0	1	100	1	10^{-4}	10	0
1	10	1	10^{-4}	100	0	1	100	1	10^{-4}	100	0
1	10	10	10^{-4}	100	<10	1	100	10	10^{-4}	100	<10
1	10	100	10^{-4}	100	<10	1	100	100	10^{-4}	100	<10
1	10	1	1	1	0	1	100	1	1	1	0
1	10	1	1	10	0	1	100	1	1	10	0
1	10	1	1	100	0	1	100	1	1	100	0

In order to provide a sufficient condition to ensure $\bar{\mathbf{U}}_i^{n+1} \in G,\ \forall i$, let $\hat{S}_i^x = \{\hat{x}_i^\beta,\ \beta = 1, \ldots, N\}$ be the Legendre Gauss–Lobatto quadrature points in I_i, with the corresponding quadrature weights $\{\hat{\omega}_\beta\}_{\beta=1}^N$ on $[-\frac{1}{2}, \frac{1}{2}]$ satisfying $\sum_{\beta=1}^N \hat{\omega}_\beta = 1$ and $\hat{\omega}_1 = \hat{\omega}_N$. Since this quadrature is exact for the integral of polynomials of degree up to $2N-3$, we take N such that $2N - 3 \geqslant k$.

Theorem 2.3. *For the scheme (2.16), suppose* $\bar{\mathbf{U}}_i^n \in G,\ \forall i$. *If* $\mathbf{U}_h(x, t_n) \in G$ *for* $\forall x \in \hat{S}_i^x,\ \forall i$, *then* $\bar{\mathbf{U}}_i^{n+1}$ *will belong to* $G, \forall i$, *under the CFL condition*

$$\lambda a_x \leqslant \alpha_0 \hat{\omega}_1. \tag{2.17}$$

Here α_0 *is the same as in Lemma 2.1.*

The proof is the same as in [27]. With this sufficient condition, a positivity-preserving limiter can be defined and analyzed. We will not include the details, but the limiter itself in Section 2.3. Though the Lax–Friedrichs numerical flux is considered in this paper, one can work with other numerical fluxes as along as the first order scheme in (2.7) combined with these numerical fluxes is positivity-preserving.

For conservative positivity-preserving DG method, the solution has the following property regarding stability.

Theorem 2.4. *Assuming vanishing, reflective, or periodic boundary conditions, then the conservative positivity-preserving DG method will satisfy*

$$||\rho_h^{n+1}||_{L^1(\Omega)} = ||\rho_h^n||_{L^1(\Omega)}, \quad ||E_h^{n+1}||_{L^1(\Omega)} = ||E_h^n||_{L^1(\Omega)}. \tag{2.18}$$

The proof can be obtained similarly as that for Theorem 2.3 in [23]. For most numerical methods solving the ideal MHD system, it is not easy to obtain provable stability. The seemly simple stability result in Theorem 2.4 ensures the L^1 stability of two conservative variables, density and the total energy, and this explains why positivity-preserving limiters tend to play a more important role to the robustness of conservative numerical methods in MHD simulations (see Section 4 and [12]). This stability result also hold for higher dimensional DG methods in Section 3.

2.2. Positivity-preserving central DG schemes

To define central DG methods, we start with a mesh $\{I_i\}_i$ of the computational domain $\Omega = (x_{min}, x_{max})$, with $I_i = (x_i, x_{i+1})$. With $x_{i+\frac{1}{2}} = \frac{1}{2}(x_i + x_{i+1})$ and $I_i^D = (x_{i-\frac{1}{2}}, x_{i+\frac{1}{2}})$, we can define a dual mesh $\{I_i^D\}_i$ for Ω. Without loss of generality, the mesh is assumed to be uniform with a meshsize Δx. Associated to these meshes, we further introduce two finite dimensional discrete spaces

$$\mathcal{U}_h = \{\mathbf{u} = (u_1, \ldots, u_8)^{\mathrm{T}} : u_l|_{I_i} \in P^k(I_i), \forall l, i\},$$
$$\mathcal{U}_h^D = \{\mathbf{u} = (u_1, \ldots, u_8)^{\mathrm{T}} : u_l|_{I_i^D} \in P^k(I_i^D), \forall l, i\},$$

which include piecewise polynomials of degree at most k with respect to each mesh. The semi-discrete central DG method for (2.3) is given as follows: look for $\mathbf{U}_h \in \mathcal{U}_h$ and $\mathbf{U}_h^D \in \mathcal{U}_h^D$ such that $\forall \mathbf{u} \in \mathcal{U}_h,\ \forall \mathbf{u}^D \in \mathcal{U}_h^D$, and $\forall i$,

$$\int_{I_i} \frac{\partial \mathbf{U}_h}{\partial t} \cdot \mathbf{u}\, dx - \frac{1}{\tau_{\max}} \int_{I_i} (\mathbf{U}_h^D - \mathbf{U}_h) \cdot \mathbf{u}\, dx - \int_{I_i} \mathbf{F}(\mathbf{U}_h^D) \cdot \frac{\partial \mathbf{u}}{\partial x}\, dx + \mathbf{F}(\mathbf{U}_h^D)_{i+1} \mathbf{u}_{i+1}^- - \mathbf{F}(\mathbf{U}_h^D)_i \mathbf{u}_i^+ = 0, \tag{2.19a}$$

$$\int_{I_i^D} \frac{\partial \mathbf{U}_h^D}{\partial t} \cdot \mathbf{u}^D\, dx - \frac{1}{\tau_{\max}} \int_{I_i^D} (\mathbf{U}_h - \mathbf{U}_h^D) \cdot \mathbf{u}^D\, dx - \int_{I_i^D} \mathbf{F}(\mathbf{U}_h) \cdot \frac{\partial \mathbf{u}^D}{\partial x}\, dx + \mathbf{F}(\mathbf{U}_h)_{i+\frac{1}{2}} \mathbf{u}_{i+\frac{1}{2}}^{D,-} - \mathbf{F}(\mathbf{U}_h)_{i-\frac{1}{2}} \mathbf{u}_{i-\frac{1}{2}}^{D,+} = 0. \tag{2.19b}$$

Here $\tau_{\max}$ is the maximum time step allowed by the CFL condition. Both $\mathbf{U}_h$ and $\mathbf{U}_h^D$ provide approximations to the exact solution $\mathbf{U}$. Different from DG methods in Section 2.1, with the use of overlapping meshes, there is no numerical flux in central DG methods.

For central DG methods in (2.19), we want to propose positivity-preserving limiters, with which the cell average of the numerical solution on each mesh belongs to the admissible set G at each discrete time t_n. To achieve this, we start with the first order central DG method using the forward Euler time discretization, given as

$$\mathbf{U}_i^{n+1} = (1-\theta)\mathbf{U}_i^n + \theta \frac{\mathbf{U}_i^{D,n} + \mathbf{U}_{i+1}^{D,n}}{2} - \lambda\Big(\mathbf{F}(\mathbf{U}_{i+1}^{D,n}) - \mathbf{F}(\mathbf{U}_i^{D,n})\Big), \tag{2.20a}$$

$$\mathbf{U}_i^{D,n+1} = (1-\theta)\mathbf{U}_i^{D,n} + \theta \frac{\mathbf{U}_i^n + \mathbf{U}_{i-1}^n}{2} - \lambda\big(\mathbf{F}(\mathbf{U}_i^n) - \mathbf{F}(\mathbf{U}_{i-1}^n)\big). \tag{2.20b}$$

Here $\lambda = \frac{\Delta t}{\Delta x}$, and $\mathbf{U}_i^n$ (resp. $\mathbf{U}_i^{D,n}$) approximates the cell average of the exact solution in I_i (resp. I_i^D) at time t_n. $\theta = \frac{\Delta t}{\tau_{\max}}$ and it can be regarded as a parameter in $[0,1]$. In real simulations θ can depend on n. It turns out that to establish the positivity-preserving property of the first order central DG method (2.20), it is sufficient to consider the case when $\theta = 1$.

Lemma 2.5. *Under Assumption $\mathcal{P}$, the first order central DG method (2.20) with $\theta = 1$ is positivity-preserving under a CFL condition*

$$\lambda a_x \leqslant \alpha_0, \tag{2.21}$$

with $\alpha_0 = \frac{1}{2}$. That is, if $\mathbf{U}_i^n, \mathbf{U}_i^{D,n} \in G, \forall i$, then $\mathbf{U}_i^{n+1}, \mathbf{U}_i^{D,n+1} \in G, \forall i$. Here a_x is defined as

$$a_x = \max(||(|u_x| + c_f^x)(\cdot, t_n)||_\infty, ||(|u_x^D| + c_f^{D,x})(\cdot, t_n)||_\infty). \tag{2.22}$$

In addition, the numerical B_x stays as constant.

Proof. It is trivial to show that the numerical B_x stays as constant. Next assume $\mathbf{U}_i^n, \mathbf{U}_i^{D,n} \in G, \forall i$, we want to show that $\mathbf{U}_i^{n+1}$ and $\mathbf{U}_i^{D,n+1}$, computed from (2.20) with $\theta = 1$, are also in $G, \forall i$.

Consider

$$\begin{cases} \frac{\partial \mathbf{U}}{\partial t} + \frac{\partial}{\partial x}\mathbf{F}(\mathbf{U}) = \mathbf{0}, \\ \mathbf{U}(x, t_n) = \mathbf{U}_i^n, \qquad \text{when } x \in I_i. \end{cases} \tag{2.23}$$

Note the eigenvalues of the Jacobian of $\mathbf{F}(\mathbf{U})$ are within $[-a_x, a_x]$. Let $t_{n+1} = t_n + \Delta t$, with $\Delta t \leqslant \frac{\Delta x}{2a_x}$. In the time interval $[t_n, t_{n+1}]$, the solution to (2.23) consists of many Riemann problems, with each stemming from $x = x_i$ at $t = t_n,\ \forall i$. Moreover, these Riemann problems will not intersect each other, therefore the exact solution $\mathbf{U}(x,t) \in G$ for $t \in [t_n, t_{n+1}]$ due to Assumption $\mathcal{P}$. If we further integrate Eq. (2.23) over the control volume $I_i^D \times [t_n, t_{n+1}]$, then

$$\tilde{\mathbf{U}}_i := \frac{1}{\Delta x}\int_{I_i^D}\mathbf{U}(x,t_{n+1})\,dx = \frac{1}{\Delta x}\int_{I_i^D}\mathbf{U}(x,t_n)\,dx - \frac{1}{\Delta x}\left(\int_{t_n}^{t_{n+1}}(\mathbf{F}(\mathbf{U}(x_{i+\frac{1}{2}},t)) - \mathbf{F}(\mathbf{U}(x_{i-\frac{1}{2}},t)))dt\right)$$
$$= \frac{\mathbf{U}_i^n + \mathbf{U}_{i-1}^n}{2} - \lambda\big(\mathbf{F}(\mathbf{U}_i^n) - \mathbf{F}(\mathbf{U}_{i-1}^n)\big). \tag{2.24}$$

Since G is a convex set, $\mathbf{U}(x,t_{n+1}) \in G$ implies $\tilde{\mathbf{U}}_i = \frac{1}{\Delta x}\int_{I_i^D}\mathbf{U}(x,t_{n+1})dx \in G$. For the last equality (2.24), we use $\mathbf{U}(x_{i-\frac{1}{2}},t) = \mathbf{U}_{i-1}^n$ and $\mathbf{U}(x_{i+\frac{1}{2}},t) = \mathbf{U}_i^n$ for $t \in (t_n,t_{n+1})$ and this is due to the self-similarity property of the solution to the Riemann problem. Now note that $\tilde{\mathbf{U}}_i$ is exactly $\mathbf{U}_i^{D,n+1}$, which is computed from (2.20b) with $\theta = 1$ and therefore also belongs to G as long as the CFL condition $\lambda a_x \leqslant \frac{1}{2}$ holds. Similarly, one can prove that $\mathbf{U}_i^{n+1}$ is in G under the same CFL condition. □

With Lemma 2.5, we are now ready for the general central DG methods (including the first order case). Since SSP time discretizations are used in this work, we only need to consider the scheme satisfied by the cell average of the central DG solution with the forward Euler time discretization, given as

$$\bar{\mathbf{U}}_i^{n+1} = (1-\theta)\bar{\mathbf{U}}_i^n + \frac{\theta}{\Delta x}\int_{I_i}\mathbf{U}_h^{D,n}\,dx - \lambda\Big(\mathbf{F}(\mathbf{U}_{i+1}^{D,n}) - \mathbf{F}(\mathbf{U}_i^{D,n})\Big), \tag{2.25a}$$

$$\bar{\mathbf{U}}_i^{D,n+1} = (1-\theta)\bar{\mathbf{U}}_i^{D,n} + \frac{\theta}{\Delta x}\int_{I_i^D}\mathbf{U}_h^{n}\,dx - \lambda\Big(\mathbf{F}(\mathbf{U}_{i+\frac{1}{2}}^{n}) - \mathbf{F}(\mathbf{U}_{i-\frac{1}{2}}^{n})\Big), \tag{2.25b}$$

Here $\bar{\mathbf{U}}_i^n$ (resp. $\bar{\mathbf{U}}_i^{D,n}$) is the cell average of $\mathbf{U}_h$ on I_i (resp. $\mathbf{U}_h^D$ on I_i^D) at time t_n. We also use $\mathbf{U}_{i-\frac{1}{2}}^n = \mathbf{U}_h(x_{i-\frac{1}{2}},t_n)$ and $\mathbf{U}_i^{D,n} = \mathbf{U}_h^D(x_i,t_n),\ \forall i$.

In order to provide a sufficient condition to ensure $\bar{\mathbf{U}}_i^{n+1}, \bar{\mathbf{U}}_i^{D,n+1} \in G, \forall i$, let $\hat{S}_i^{1,x} = \{\hat{x}_i^{1,\beta},\ \beta = 1,\dots,N\}$ and $\hat{S}_i^{2,x} = \{\hat{x}_i^{2,\beta}, \beta = 1,\dots,N\}$ be the Legendre Gauss–Lobatto quadrature points on $[x_i, x_{i+1/2}]$ and $[x_{i+1/2}, x_{i+1}]$, respectively. The corresponding quadrature rule is exact for the integral of polynomials of degree up to $2N-3$. We choose N such that $2N-3 \geqslant k$. Let $\hat{\omega}_\beta,\ \beta = 1,\dots N$ be the Legendre Gauss–Lobatto quadrature weights for the interval $[-\frac{1}{2},\ \frac{1}{2}]$. Note that $\sum_{\beta=1}^N \hat{\omega}_\beta = 1,\ \hat{\omega}_1 = \hat{\omega}_N$. And $x_i = \hat{x}_i^{1,1} = \hat{x}_{i-1}^{2,N},\ x_{i+\frac{1}{2}} = \hat{x}_i^{1,N} = \hat{x}_i^{2,1},\ \forall i$.

Theorem 2.6. *For the scheme (2.25), suppose $\bar{\mathbf{U}}_i^n, \bar{\mathbf{U}}_i^{D,n} \in G, \forall i$. If $\mathbf{U}_h(x,t_n), \mathbf{U}_h^D(x,t_n) \in G$ for $\forall x \in \hat{S}_i^{l,x}, \forall i$ and $l = 1,2$, then $\bar{\mathbf{U}}_i^{n+1}$ and $\bar{\mathbf{U}}_i^{D,n+1}$ will belong to $G, \forall i$, under the CFL condition*

$$\lambda a_x \leqslant \theta\alpha_0\hat{\omega}_1. \tag{2.26}$$

Here α_0 is the same as in Lemma 2.5.

Proof. Using the Legendre Gauss–Lobatto quadrature rule, we have

$$\frac{1}{\Delta x}\int_{I_i}\mathbf{U}_h^{D,n}dx = \frac{1}{2}\left(\sum_{\beta=1}^N\hat{\omega}_\beta\mathbf{U}_{1,\beta}^D + \sum_{\beta=1}^N\hat{\omega}_\beta\mathbf{U}_{2,\beta}^D\right),$$

where $\mathbf{U}_{l,\beta}^D = \mathbf{U}_h^{D,n}(\hat{x}_i^{l,\beta}),\ l = 1,2$. Now

$$\bar{\mathbf{U}}_i^{n+1} = (1-\theta)\bar{\mathbf{U}}_i^n + \frac{\theta}{\Delta x}\int_{I_i}\mathbf{U}_h^{D,n}\,dx - \lambda\Big(\mathbf{F}(\mathbf{U}_{i+1}^{D,n}) - \mathbf{F}(\mathbf{U}_i^{D,n})\Big), \tag{2.27}$$

$$= (1-\theta)\bar{\mathbf{U}}_i^n + \frac{\theta}{2}\left(\sum_{\beta=1}^N\hat{\omega}_\beta\mathbf{U}_{1,\beta}^D + \sum_{\beta=1}^N\hat{\omega}_\beta\mathbf{U}_{2,\beta}^D\right) - \lambda\Big(\mathbf{F}(\mathbf{U}_{i+1}^{D,n}) - \mathbf{F}(\mathbf{U}_i^{D,n})\Big) \tag{2.28}$$

$$= (1-\theta)\bar{\mathbf{U}}_i^n + \frac{\theta}{2}\left(\sum_{\beta=2}^N\hat{\omega}_\beta\mathbf{U}_{1,\beta}^D + \sum_{\beta=1}^{N-1}\hat{\omega}_\beta\mathbf{U}_{2,\beta}^D\right) + \theta\hat{\omega}_1\tilde{\mathbf{U}}_i \tag{2.29}$$

with $\tilde{\mathbf{U}}_i = \frac{\mathbf{U}_i^{D,n}+\mathbf{U}_{i+1}^{D,n}}{2} - \frac{\lambda}{\theta\hat{\omega}_1}\Big(\mathbf{F}(\mathbf{U}_{i+1}^{D,n}) - \mathbf{F}(\mathbf{U}_i^{D,n})\Big)$. We here use $\hat{\omega}_1 = \hat{\omega}_N,\ \mathbf{U}_{1,1}^D = \mathbf{U}_i^{D,n}$, and $\mathbf{U}_{2,N}^D = \mathbf{U}_{i+1}^{D,n}$. From Lemma 2.5, we know $\tilde{\mathbf{U}}_i \in G$ as long as $\frac{\lambda}{\theta\hat{\omega}_1}a_x \leqslant \alpha_0$, namely $\lambda a_x \leqslant \theta\alpha_0\hat{\omega}_1$. Note that $\bar{\mathbf{U}}_i^{n+1}$ is a convex combination of $\bar{\mathbf{U}}_i^n$, $\mathbf{U}_{1,\beta}^D$ with $\beta = 2,\dots,N,\ \mathbf{U}_{2,\beta}^D$ with $\beta = 1,\dots,N-1$ and $\tilde{\mathbf{U}}_i$, which all belong to the convex admissible set G, therefore $\bar{\mathbf{U}}_i^{n+1} \in G,\ \forall i$. Similarly, one can show $\bar{\mathbf{U}}_i^{D,n+1} \in G,\ \forall i$. □

For positivity-preserving central DG method, the solution has the following property regarding L^1 stability of density and total energy. The proof can be obtained similarly as that for Theorem 2.3 in [23].

Theorem 2.7. *Assuming vanishing, reflective, or periodic boundary conditions, then the positivity-preserving central DG method will satisfy*

$$||\rho_h^{n+1}||_{L^1(\Omega)} + ||\rho_h^{D,n+1}||_{L^1(\Omega)} = ||\rho_h^n||_{L^1(\Omega)} + ||\rho_h^{D,n}||_{L^1(\Omega)},$$
$$||E_h^{n+1}||_{L^1(\Omega)} + ||E_h^{D,n+1}||_{L^1(\Omega)} = ||E_h^n||_{L^1(\Omega)} + ||E_h^{D,n}||_{L^1(\Omega)}.$$

Compared with DG methods, there are twice as many quadrature points used in Theorem 2.6 for central DG methods. Unlike DG methods, the CFL condition to ensure the positivity-preserving property of central DG methods also depends on the value of θ which cannot be zero. Such dependence on θ is expected, as when the first order central DG method (2.20) is applied to a scalar conservation law $u_t + f(u)_x = 0$, it can be verified algebraically that,

$$\lambda \max |f'(u)| \leqslant \theta\alpha_0, \text{ with } \alpha_0 = \frac{1}{2} \text{ and } 0 < \theta < 1$$

is the sufficient and necessary condition for (2.20) to be a monotone scheme, which is known to satisfy the strict maximum principle. Furthermore, the fact that central DG methods does not involve any numerical flux implies that one can not work with various first order positivity-preserving building blocks as in the DG framework by applying different numerical fluxes.

2.3. Positivity-preserving limiters

With the developments in Sections 2.1 and 2.2, in this section we present a positivity-preserving limiter based on the work in [27] for compressible Euler equations and its recent improvement in [23] for reactive Euler equations.

For DG method, let K represent a mesh element I_i with any point as $\mathbf{x}$, let S_K represent the set of relevant quadrature points in K, namely $S_K = \hat{S}_i^x$. Given the DG solution polynomial $\mathbf{U}_K = (\rho, \mathbf{m}^T, \mathbf{B}^T, E)^{\mathrm{T}}$ in K at time t_n, with the cell average $\bar{\mathbf{U}}_K = (\bar{\rho}, \bar{\mathbf{m}}^T, \bar{\mathbf{B}}^T, \bar{E})^{\mathrm{T}}$ belongs to the admissible set G, we will define a positivity-preserving limiter to modify $\mathbf{U}_K$ into $\tilde{\mathbf{U}}_K$, such that $\tilde{\mathbf{U}}_K$ not only keeps the accuracy and local conservation property of $\mathbf{U}_K$ ([27]), but also satisfies the positivity property, namely $\tilde{\mathbf{U}}_K(\mathbf{x}) \in G$ for any $\mathbf{x} \in S_K$. With this $\tilde{\mathbf{U}}_K$ used in the DG method (2.6), the cell average of the solution at t_{n+1} will be in G with the forward Euler method time discretization under the CFL condition $\lambda a_x \leqslant \alpha_0\hat{\omega}_1$.

Following [27,23], the positivity-preserving limiter for DG method is given as follows. With the forward Euler time discretization, on each mesh element K,

1. We first enforce the positivity of density, by modifying ρ into $\hat{\rho} = \hat{\eta}_K(\rho - \bar{\rho}) + \bar{\rho}$, with $\hat{\eta}_K = \min_{\mathbf{x}\in S_K}\{1, |(\bar{\rho} - \epsilon)/(\bar{\rho} - \rho(\mathbf{x}))|\}$. Here ϵ is a small number such that $\min_K \bar{\rho}_K > \epsilon$. In practice, we take $\epsilon = 10^{-13}$.
2. Next we enforce the positivity of pressure. Define $\hat{\mathbf{U}}_K = (\hat{\rho}, \mathbf{m}^T, \mathbf{B}^T, E)^{\mathrm{T}}$. For any $\mathbf{x} \in S_K$, if $p(\hat{\mathbf{U}}_K(\mathbf{x})) \geqslant 0$ we set $\eta_{\mathbf{x}} = 1$; otherwise

$$\eta_{\mathbf{x}} = \frac{p(\bar{\mathbf{U}}_K)}{p(\bar{\mathbf{U}}_K) - p(\hat{\mathbf{U}}_K)}. \tag{2.30}$$

We now define $\tilde{\mathbf{U}}_K = \eta_K(\hat{\mathbf{U}}_K - \bar{\mathbf{U}}_K) + \bar{\mathbf{U}}_K$, with $\eta_K = \min_{\mathbf{x}\in S_K}\eta_{\mathbf{x}}$.

It is easy to see $\hat{\rho}$ is positive. For pressure, with $p(\mathbf{U})$ being concave (when $\rho > 0$) and based on a similar argument as in [23], one has

$$p(\tilde{\mathbf{U}}_K) = p(\eta_K(\hat{\mathbf{U}}_K - \bar{\mathbf{U}}_K) + \bar{\mathbf{U}}_K) = p(\eta_K(\hat{\mathbf{U}}_K) + (1-\eta_K)\bar{\mathbf{U}}_K) \geqslant \eta_K p(\hat{\mathbf{U}}_K) + (1-\eta_K)p(\bar{\mathbf{U}}_K), \ (\rho(\hat{\mathbf{U}}_K) > 0, \rho(\bar{\mathbf{U}}_k) > 0, \text{ Jensens inequality}) \tag{2.31}$$

For any $\mathbf{x} \in S_K$, if $p(\hat{\mathbf{U}}_K(\mathbf{x})) \geqslant 0$, there is $p(\tilde{\mathbf{U}}_K(\mathbf{x})) \geqslant 0$ according to (2.31). If instead $p(\hat{\mathbf{U}}_K(\mathbf{x})) < 0$, then $p(\hat{\mathbf{U}}_K(\mathbf{x})) - p(\bar{\mathbf{U}}_K) < 0$, if we further use $\eta_{\mathbf{x}}$ defined in (2.30), there will be

$$p(\tilde{\mathbf{U}}_K(\mathbf{x})) \geqslant \eta_K p(\hat{\mathbf{U}}_K(\mathbf{x})) + (1-\eta_K)p(\bar{\mathbf{U}}_K) = \eta_K(p(\hat{\mathbf{U}}_K(\mathbf{x})) - p(\bar{\mathbf{U}}_K)) + p(\bar{\mathbf{U}}_K) \geqslant \eta_{\mathbf{x}}(p(\hat{\mathbf{U}}_K(\mathbf{x})) - p(\bar{\mathbf{U}}_K)) + p(\bar{\mathbf{U}}_K) = 0.$$

For central DG method, given the central DG solution polynomials $\mathbf{U}_h$ and $\mathbf{U}_h^D$ at time t_n, with the cell averages in the set G, we will give a positivity-preserving limiter which modify $\mathbf{U}_h$ and $\mathbf{U}_h^D$ into $\tilde{\mathbf{U}}_h$ and $\tilde{\mathbf{U}}_h^D$ such that they will satisfy the sufficient condition in Theorem 2.6, while maintaining accuracy and local conservation. In fact, this limiter is almost the same as above for DG methods, as long as it is applied to $\mathbf{U}_h$ and $\mathbf{U}_h^D$ separately and the notations K and S_K are re-defined as follows: On the primal mesh, let K represent a mesh element I_i. Let S_K represent the set of relevant quadrature points in K, namely $S_K = \hat{S}_i^{1,x} \cup \hat{S}_i^{2,x}$. On the dual mesh, let K represent a mesh element I_i^D. Let S_K represent the set of relevant quadrature points in K, namely $S_K = \hat{S}_i^{1,x} \cup \hat{S}_{i-1}^{2,x}$. The numerical solution on K is denoted as $\mathbf{U}_K$. One can see that the total number quadrature points involved in the positivity-preserving limiter for central DG methods is twice ($2d$ with d being the spatial dimension) of that of standard DG methods.

For SSP time discretizations, the limiter will be used after each stage for multi-stage methods or in each step for multi-step methods.

Remark 2.8. Though the positivity-preserving limiter improves the stability of the numerical methods, it is insufficient to ensure the stability of the overall algorithm, for which we still need to apply nonlinear limiters ([27]). In our simulations, the minmod TVB limiter is applied right before the positivity-preserving limiter.

Remark 2.9. When enforcing the positivity of the pressure in the second step, we follow the improved technique proposed in [23] for its simplicity and robustness. Alternatively, one can use the procedure in Section 2.2 of [27] which will reply on finding the roots of a cubic polynomial at each relevant quadrature point. Our numerical experiments show that this more involved procedure is less robust, as indicated in [23].

3. Two-dimensional case

In two dimensions when all unknown functions depend on spatial variables x and y, Eqs. (1.1a)–(1.1d) can be written as

$$\frac{\partial \mathbf{U}}{\partial t}+\frac{\partial}{\partial x}\mathbf{F}_1(\mathbf{U})+\frac{\partial}{\partial y}\mathbf{F}_2(\mathbf{U})=\mathbf{0}, \tag{3.32}$$

where $\mathbf{F}_1$ is the same as $\mathbf{F}$ in one dimension and

$$\mathbf{F}_2(\mathbf{U})=\left(m_y,\frac{m_xm_y}{\rho}-B_yB_x,\frac{m_y^2}{\rho}+p+\frac{1}{2}|\mathbf{B}|^2-B_y^2,\frac{m_ym_z}{\rho}-B_yB_z,\frac{m_yB_x-m_xB_y}{\rho},0,\frac{m_yB_z-m_zB_y}{\rho},\frac{1}{\rho}\left(m_y\left(E+p+\frac{1}{2}|\mathbf{B}|^2\right)-B_y\mathbf{m}\cdot\mathbf{B}\right)\right)^{\mathrm{T}}.$$

In [27] when the compressible Euler system is considered, positivity-preserving limiters for higher spatial dimensions on Cartesian meshes can be devised as long as a first order positivity-preserving DG method is available in one spatial dimension. However for the ideal MHD system, the situation is different due to the nonzero *numerical* divergence in two dimensions. This implies that the numerically relevant Riemann problems are not the same for one and higher spatial dimensions. The one-dimensional Riemann problem starts with the initial data where B_x is constant throughout the domain, while for higher than one dimension, the numerically relevant Riemann problem allows a nonzero divergence of $\mathbf{B}$ hence a nontrivial jump in the normal component of $\mathbf{B}$. On the Cartesian mesh, this implies B_x (resp. B_y) is not necessary to be continuous in x-direction (resp. y-direction). For such Riemann problem, one can not make an assumption similar to Assumption $\mathcal{P}$, therefore can not establish the positivity-preserving property of the first order DG or central DG method as in Lemmas 2.1 and 2.5. On the other hand, if the first order building block is positivity-preserving, then necessary conditions similar to Theorems 2.3 and 2.6 can be established for high order DG and central DG methods to ensure the cell averages of their solutions belong to G. This motivates us to still state the "necessary conditions" and provide the "positivity-preserving" limiters. One should be aware that these necessary conditions hence the limiters are given formally without any rigorous proof. Their actual performance in terms of stability and effectiveness in preserving positivity will be illustrated by numerical experiments in Section 4.

3.1. DG methods

To define the DG methods, we start with a mesh $\{I_{ij}\}_{i,j}$ for the computational domain $\Omega=(x_{\min},x_{\max})\times(y_{\min},y_{\max})$, with $I_{ij}=I_i\times J_j=(x_i,x_{i+1})\times(y_j,y_{j+1})$. Without loss of generality, the mesh is assumed to be uniform with mesh sizes Δx and Δy. We further define a finite dimensional space

$$\mathcal{U}_h=\{\mathbf{u}=(u_1,u_2,\ldots,u_8)^{\mathrm{T}}:u_l|_{I_{ij}}\in P^k(I_{ij}),\forall l,i,j\}. \tag{3.33}$$

Now the standard semi-discrete DG methods for (3.32) can be given as follows: look for $\mathbf{U}_h\in\mathcal{U}_h$, such that $\forall\mathbf{u}\in\mathcal{U}_h$, and $\forall i,j$,

$$\begin{aligned}&\int_{I_{ij}}\frac{\partial \mathbf{U}_h}{\partial t}\cdot\mathbf{u}\,dx\,dy-\int_{I_{ij}}\left(\mathbf{F}_1(\mathbf{U}_h)\cdot\frac{\partial \mathbf{u}}{\partial x}+\mathbf{F}_2(\mathbf{U}_h)\cdot\frac{\partial \mathbf{u}}{\partial y}\right)dx\,dy+\int_{J_j}(\mathbf{h}_1\mathbf{u}^-)|_{x=x_{i+1}}-(\mathbf{h}_1\mathbf{u}^+)|_{x=x_i}dy+\int_{I_i}(\mathbf{h}_2\mathbf{u}^-)|_{y=y_{j+1}}\\&\quad-(\mathbf{h}_2\mathbf{u}^+)|_{y=y_j}dx=0.\end{aligned} \tag{3.34}$$

Here, $\mathbf{h}_1(\cdot,\cdot)$ (resp. $\mathbf{h}_2(\cdot,\cdot)$) is the numerical flux in y-direction (resp. x-direction) mesh interfaces. The integrals in (3.34) (except the first one) are further approximated by quadratures with sufficient accuracy [8]. For the numerical flux, the simple Lax–Friedrichs flux

$$\mathbf{h}_1(\mathbf{u}^-,\mathbf{u}^+)=\frac{1}{2}(\mathbf{F}_1(\mathbf{u}^-)+\mathbf{F}_1(\mathbf{u}^+)-a_x(\mathbf{u}^+-\mathbf{u}^-)), \tag{3.35a}$$

$$\mathbf{h}_2(\mathbf{u}^-,\mathbf{u}^+)=\frac{1}{2}(\mathbf{F}_2(\mathbf{u}^-)+\mathbf{F}_2(\mathbf{u}^+)-a_y(\mathbf{u}^+-\mathbf{u}^-)), \tag{3.35b}$$

is used, where $a_x=||(|u_x|+c_f^x)(\cdot,\cdot,t)||_\infty$ and $a_y=||(|u_y|+c_f^y)(\cdot,\cdot,t)||_\infty$ with c_f^x and c_f^y being the fast speed in x and y directions, respectively.

With the forward Euler method as the time discretization, the cell average of the DG solution, $\bar{\mathbf{U}}_{ij}^n$ satisfies

$$\bar{\mathbf{U}}_{ij}^{n+1} = \bar{\mathbf{U}}_{ij}^n + \frac{\Delta t}{\Delta x \Delta y}\left(\int_{J_j} \mathbf{h}_1\Big|_{x=x_i}^{x=x_{i+1}} dy + \int_{I_i} \mathbf{h}_2\Big|_{y=y_j}^{y=y_{j+1}} dx\right) \tag{3.36}$$

In order to state the "sufficient condition" for $\bar{\mathbf{U}}_{ij}^{n+1}$ to belong to G (defined in 2.4), let $\hat{S}_i^x = \{\hat{x}_i^\beta,\ \beta = 1,\ldots,N\}$ and $\hat{S}_j^y = \{\hat{y}_j^\beta,\ \beta = 1,\ldots,N\}$ be the Legendre Gauss–Lobatto quadrature points on I_i and J_j, respectively, with the corresponding quadrature weights $\{\hat{\omega}_\beta\}_{\beta=1}^N$ on $[-\frac{1}{2}, \frac{1}{2}]$ satisfying $\sum_{\beta=1}^N \hat{\omega}_\beta = 1$ and $\hat{\omega}_1 = \hat{\omega}_N$. We take N such that $2N-3 \geqslant k$. Let $S_i^x = \{x_i^\alpha, : \alpha = 1,\ldots,L\}$ and $S_j^y = \{y_j^\alpha, : \alpha = 1,\ldots,L\}$ be the Gaussian quadrature points on I_i and J_j, respectively. L is chosen such that the Gaussian quadrature is exact for the integral of single variable polynomials of degree $2k+1$. Define

$$S_{ij} = (S_i^x \otimes \hat{S}_j^y) \cup (\hat{S}_i^x \otimes S_j^y).$$

''Sufficient condition'' for DG methods in two dimensions. *For the scheme (3.36), given $\bar{\mathbf{U}}_{ij}^n$ in $G, \forall i,j$. If $\mathbf{U}_h(x,y,t_n) \in G$ for $\forall (x,y) \in S_{ij}, \forall i,j$, and if the integrals on the mesh interfaces in (3.34) (and therefore (3.36)) are approximated by Gauss quadrature with S_i^x or S_j^y given above, then under the CFL condition*

$$\lambda_x a_x + \lambda_y a_y \leqslant \alpha_0 \hat{\omega}_1, \tag{3.37}$$

$\bar{\mathbf{U}}_{ij}^{n+1}$ will belong to $G, \forall i,j$. Here α_0 is some constant.

Based on [27], in order to rigorously prove these sufficient conditions, one can try to show that the first order DG method with the Lax–Friedrichs numerical flux in (2.7)–(2.9) is positivity-preserving under some CFL condition *when B_x is piecewise constant*. Though one can not make Assumption $\mathcal{P}$ with discontinuity in B_x, we carry out some numerical experiments in Appendix A as in Section 2.1.1 to seek some numerical evidence. Our results in Tables A.7 and A.8 demonstrate numerically that the first order DG method with the Lax–Friedrichs numerical flux is positivity-preserving under the CFL condition (2.10) with $\alpha = \frac{1}{2}$.

3.2. Central DG methods

To define central DG methods, besides the mesh $\{I_{ij}\}_{i,j}$ and the discrete space $\mathcal{U}_h$ as introduced for DG methods, one also needs a dual mesh $\{I_{ij}^D\}_{i,j}$ and its associated discrete space $\mathcal{U}_h^D$ on it. That is, with $x_{i+\frac{1}{2}} = \frac{1}{2}(x_i + x_{i+1}), y_{j+\frac{1}{2}} = \frac{1}{2}(y_j + y_{j+1})$, we define $I_{ij}^D = I_i^D \times J_j^D = \left(x_{i-\frac{1}{2}}, x_{i+\frac{1}{2}}\right) \times \left(y_{j-\frac{1}{2}}, y_{j+\frac{1}{2}}\right)$, and

$$\mathcal{U}_h^D = \{\mathbf{u} = (u_1, u_2, \ldots, u_8)^{\mathrm{T}} : u_l|_{I_{ij}^D} \in P^k(I_{ij}^D), \forall l,i,j\}. \tag{3.38}$$

The semi-discrete central DG methods for (3.32) can be given as follows: look for $\mathbf{U}_h \in \mathcal{U}_h, \mathbf{U}_h^D \in \mathcal{U}_h^D$, such that $\forall \mathbf{u} \in \mathcal{U}_h, \forall \mathbf{u}^D \in \mathcal{U}_h^D$, and $\forall i,j$,

$$\int_{I_{ij}} \frac{\partial \mathbf{U}_h}{\partial t} \cdot \mathbf{u} dx dy - \frac{1}{\tau_{\max}} \int_{I_{ij}} (\mathbf{U}_h^D - \mathbf{U}_h) dx dy - \int_{I_{ij}} \left(\mathbf{F}_1(\mathbf{U}_h^D) \cdot \frac{\partial \mathbf{u}}{\partial x} + \mathbf{F}_2(\mathbf{U}_h^D) \cdot \frac{\partial \mathbf{u}}{\partial y}\right) dx dy + \int_{J_j} (\mathbf{F}_1(\mathbf{U}_h^D)\mathbf{u}^-)|_{x=x_{i+1}}$$
$$- (\mathbf{F}_1(\mathbf{U}_h^D)\mathbf{u}^+)|_{x=x_i} dy + \int_{I_i} (\mathbf{F}_2(\mathbf{U}_h^D)\mathbf{u}^-)|_{y=y_{j+1}} - (\mathbf{F}_2(\mathbf{U}_h^D)\mathbf{u}^+)|_{y=y_j} dx = 0,$$

Table A.7
To verify the positivity-preserving property of the first order Lax-Fredrichs DG method (2.7)–(2.9). u_x, u_y, u_z, B_y, B_z is from $U(-\gamma_1, \gamma_1)$, ρ is from $U(0, \gamma_2)$, p is from $U(0, \gamma_3)$, and B_x is from $U(-\gamma_4, \gamma_4)$. † = the total number of occurrence of negative pressure in 10^5 random experiments. *The CFL number is $\lambda_x a_x = \alpha_0 = 1/2$, B_x is discontinuous.*

α_0	γ_1	γ_2	γ_3	γ_4	†	α_0	γ_1	γ_2	γ_3	γ_4	†
1/2	10	10^{-4}	10^{-4}	1	0	1/2	100	10^{-4}	10^{-4}	1	0
1/2	10	10^{-4}	10^{-4}	10	0	1/2	100	10^{-4}	10^{-4}	10	0
1/2	10	10^{-4}	10^{-4}	100	0	1/2	100	10^{-4}	10^{-4}	100	0
1/2	10	10^{-4}	1	1	0	1/2	100	10^{-4}	1	1	0
1/2	10	10^{-4}	1	10	0	1/2	100	10^{-4}	1	10	0
1/2	10	10^{-4}	1	100	0	1/2	100	10^{-4}	1	100	0
1/2	10	1	10^{-4}	1	0	1/2	100	1	10^{-4}	1	0
1/2	10	1	10^{-4}	10	0	1/2	100	1	10^{-4}	10	0
1/2	10	1	10^{-4}	100	0	1/2	100	1	10^{-4}	100	0
1/2	10	1	1	1	0	1/2	100	1	1	1	0
1/2	10	1	1	10	0	1/2	100	1	1	10	0
1/2	10	1	1	100	0	1/2	100	1	1	100	0
1/2	100	1	10^{-4}	1000	0	1/2	100	100	10^{-4}	10,000	0
1/2	100	100	10^{-4}	1000	0	1/2	100	100	10^{-4}	100,000	0

Table A.8
To verify the positivity-preserving property of the first order Lax-Fredrichs DG method (2.7)–(2.9). u_x, u_y, u_z, B_y, B_z is from $U(-\gamma_1, \gamma_1)$, ρ is from $U(0, \gamma_2)$, p is from $U(0, \gamma_3)$, and B_x is from $U(-\gamma_4, \gamma_4)$. † = the total number of occurrence of negative pressure in 10^5 random experiments. *The CFL number is* $\lambda_x a_x = \alpha_0 > 1/2$, B_x *is discontinuous.*

α_0	γ_1	γ_2	γ_3	γ_4	†	α_0	γ_1	γ_2	γ_3	γ_4	†
3/5	10	1	10^{-4}	100	0	3/5	100	1	10^{-4}	100	0
3/5	10	10	10^{-4}	100	0	3/5	100	100	10^{-4}	100	0
3/5	10	1	1	100	0	3/5	100	1	1	100	0
4/5	10	1	10^{-4}	100	<10	4/5	100	1	1	10	0
4/5	10	10	10^{-4}	100	<10	4/5	100	1	1	100	<10
1	10	10^{-4}	1	1	0	1	100	10^{-4}	1	1	0
1	10	10^{-4}	1	10	0	1	100	10^{-4}	1	10	0
1	10	10^{-4}	1	100	<100	1	100	10^{-4}	1	100	0
1	10	1	10^{-4}	1	<10	1	100	1	10^{-4}	1	0
1	10	10	10^{-4}	1	<100	1	100	10	10^{-4}	1	0
1	10	100	10^{-4}	1	<100	1	100	100	10^{-4}	1	0
1	10	1	1	1	<10	1	100	1	1	1	0
1	10	1	1	10	<500	1	100	1	1	10	<10
1	10	1	1	100	<2000	1	100	1	1	100	<500
1	10	10^{-4}	10^{-4}	1	0	1	100	1	10^{-4}	10	<10
1	10	10^{-4}	10^{-4}	10	<10	1	100	10	10^{-4}	10	<30
1	10	10^{-4}	10^{-4}	100	<100	1	100	100	10^{-4}	10	<50
1	10	1	10^{-4}	10	<500	1	100	10	10^{-4}	100	<300
1	10	1	10^{-4}	100	<2000	1	100	100	10^{-4}	100	<300
1	10	10	10^{-4}	10	<500	1	100	10	1	1	0
1	10	10	10^{-4}	100	<2000	1	100	100	1	1	0

$$\int_{I_{ij}^D} \frac{\partial \mathbf{U}_h^D}{\partial t} \cdot \mathbf{u}^D \, dx\, dy - \frac{1}{\tau_{\max}} \int_{I_{ij}^D} (\mathbf{U}_h - \mathbf{U}_h^D)\, dx\, dy - \int_{I_{ij}^D} \left(\mathbf{F}_1(\mathbf{U}_h) \cdot \frac{\partial \mathbf{u}^D}{\partial x} + \mathbf{F}_2(\mathbf{U}_h) \cdot \frac{\partial \mathbf{u}^D}{\partial y} \right) dx\, dy$$
$$+ \int_{J_j^D} (\mathbf{F}_1(\mathbf{U}_h)\mathbf{u}^{D,-})|_{x=x_{i+\frac{1}{2}}} - (\mathbf{F}_1(\mathbf{U}_h)\mathbf{u}^{D,+})|_{x=x_{i-\frac{1}{2}}} dy + \int_{I_i^D} (\mathbf{F}_2(\mathbf{U}_h)\mathbf{u}^{D,-})|_{y=y_{j+\frac{1}{2}}} - (\mathbf{F}_2(\mathbf{U}_h)\mathbf{u}^{D,+})|_{y=y_{j-\frac{1}{2}}} dx = 0. \tag{3.39}$$

With the forward Euler method as the time discretization, the cell average of the central DG method, $\bar{\mathbf{U}}_{ij}^n, \bar{\mathbf{U}}_{ij}^{D,n}$ satisfies

$$\bar{\mathbf{U}}_{ij}^{n+1} = (1-\theta)\bar{\mathbf{U}}_{ij}^n + \frac{\theta}{\Delta x \Delta y} \int_{I_{ij}} \mathbf{U}_h^{D,n} dx dy - \frac{\Delta t}{\Delta x \Delta y} \left(\int_{J_j} \mathbf{F}_1(\mathbf{U}_h^{D,n}) \Big|_{x=x_i}^{x=x_{i+1}} dx + \int_{I_i} \mathbf{F}_2(\mathbf{U}_h^{D,n}) \Big|_{y=y_j}^{y=y_{j+1}} dy \right), \tag{3.40a}$$

$$\bar{\mathbf{U}}_{ij}^{D,n+1} = (1-\theta)\bar{\mathbf{U}}_{ij}^{D,n} + \frac{\theta}{\Delta x \Delta y} \int_{I_{ij}^D} \mathbf{U}_h^n dx dy - \frac{\Delta t}{\Delta x \Delta y} \left(\int_{J_j^D} \mathbf{F}_1(\mathbf{U}_h^n) \Big|_{x=x_{i-\frac{1}{2}}}^{x=x_{i+\frac{1}{2}}} dx + \int_{I_i^D} \mathbf{F}_2(\mathbf{U}_h^n) \Big|_{y=y_{j-\frac{1}{2}}}^{y=y_{j+\frac{1}{2}}} dy \right). \tag{3.40b}$$

Here $\theta = \frac{\Delta t}{\tau_{\max}}$, which can be treated as a parameter in $(0, 1]$.

In order to state the "sufficient condition" for $\bar{\mathbf{U}}_{ij}^{n+1}, \bar{\mathbf{U}}_{ij}^{D,n+1}$ from (3.40) belongs to G, let $\hat{S}_i^{1,x} = \{\hat{x}_i^{1,\beta},: \beta = 1, \ldots, N\}$ and $\hat{S}_i^{2,x} = \{\hat{x}_i^{2,\beta},: \beta = 1, \ldots, N\}$ denote the Legendre Gauss–Lobatto quadrature points on $[x_i, x_{i+1/2}]$ and $[x_{i+1/2}, x_{i+1}]$, respectively, $\hat{S}_j^{1,y} = \{\hat{y}_j^{1,\beta},: \beta = 1, \ldots, N\}$ and $\hat{S}_j^{2,y} = \{\hat{y}_j^{2,\beta},: \beta = 1, \ldots, N\}$ denote the Legendre Gauss–Lobatto quadrature points on $[y_j, y_{j+1/2}]$ and $[y_{j+1/2}, y_{j+1}]$, respectively. The corresponding quadrature weights on $[-\frac{1}{2}, \frac{1}{2}]$ are $\hat{\omega}_\beta, \beta = 1, \ldots, N$, and N is chosen such that $2N - 3 \geqslant k$. In addition, let $S_i^{1,x} = \{x_i^{1,\alpha},: \alpha = 1, \ldots, L\}$ and $S_i^{2,x} = \{x_i^{2,\alpha},: \alpha = 1, \ldots, L\}$ denote the Gaussian quadrature points on $[x_i, x_{i+1/2}]$ and $[x_{i+1/2}, x_{i+1}]$, respectively, $S_j^{1,y} = \{y_j^{1,\alpha},: \alpha = 1, \ldots, L\}$ and $S_j^{2,y} = \{y_j^{2,\alpha},: \alpha = 1, \ldots, L\}$ denote the Gaussian quadrature points on $[y_j, y_{j+1/2}]$ and $[y_{j+1/2}, y_{j+1}]$, respectively. The corresponding quadrature weights on $[-\frac{1}{2}, \frac{1}{2}]$ are $\omega_\alpha, \alpha = 1, \ldots, L$, and L is chosen such that the Gaussian quadrature is exact for the integral of single variable polynomials of degree $2k + 1$. Define

$$S_{i,j}^{l,m} = (S_i^{l,x} \otimes \hat{S}_j^{m,y}) \cup (\hat{S}_i^{l,x} \otimes S_j^{m,y})$$

with $l, m = 1, 2$.

''Sufficient condition'' for central DG methods in two dimensions. *For the scheme (3.40), given* $\bar{\mathbf{U}}_{ij}^n$ *and* $\bar{\mathbf{U}}_{ij}^{D,n}$ *in* $G, \forall i, j$ *. If* $\mathbf{U}_h(x, y, t_n), \mathbf{U}_h^D(x, y, t_n) \in G$ *for* $\forall (x, y) \in S_{i,j}^{l,m}, \forall i, j$ *and* $l, m = 1, 2$*, and if integrals on the mesh interfaces in (3.39) are approximated by*

$$\int_{J_j} \mathbf{F}_1(\mathbf{U}_h^{D,n})|_{x=x_i} dx \approx \frac{\Delta y}{2} \sum_{\alpha=1}^{L} \sum_{m=1}^{2} \mathbf{F}_1(\mathbf{U}_h^{D,n}(x_i, y_j^{m,\alpha})) \omega_\alpha,$$

$$\int_{I_i} \mathbf{F}_2(\mathbf{U}_h^{D,n})|_{y=y_j} dy \approx \frac{\Delta x}{2} \sum_{\alpha=1}^{L} \sum_{m=1}^{2} \mathbf{F}_2(\mathbf{U}_h^{D,n}(x_i^{m,\alpha}, y_j))\omega_\alpha,$$

$$\int_{J_j^D} \mathbf{F}_1(\mathbf{U}_h^n)|_{x=x_{i+\frac{1}{2}}} dx \approx \frac{\Delta y}{2} \sum_{\alpha=1}^{L} \left\{ \mathbf{F}_1(\mathbf{U}_h^n(x_{i+\frac{1}{2}}, y_{j-1}^{2,\alpha})) + \mathbf{F}_1(\mathbf{U}_h^n(x_{i+\frac{1}{2}}, y_j^{1,\alpha})) \right\} \omega_\alpha,$$

$$\int_{I_i^D} \mathbf{F}_2(\mathbf{U}_h^n)|_{y=y_{j+\frac{1}{2}}} dy \approx \frac{\Delta x}{2} \sum_{\alpha=1}^{L} \left\{ \mathbf{F}_2(\mathbf{U}_h^n(x_{i-1}^{2,\alpha}, y_{j+\frac{1}{2}})) + \mathbf{F}_2(\mathbf{U}_h^n(x_i^{1,\alpha}, y_{j+\frac{1}{2}})) \right\} \omega_\alpha,$$

for any i,j, then under the CFL condition

$$\lambda_x a_x + \lambda_y a_y \leqslant \theta \alpha_0 \hat{\omega}_1, \tag{3.41}$$

$\bar{\mathbf{W}}_{ij}^{n+1}$ and $\bar{\mathbf{W}}_{ij}^{D,n+1}$ *will belong to $G, \forall i,j$. Here α_0 is some constant.*

In both the current and previous sections, there is a un-specified constant α_0 in the sufficient conditions for both DG and central DG methods. We use $\alpha_0 = 1$ for DG methods and $\alpha_0 = 1/2$ for central DG methods in the numerical tests. In [27], a sufficient condition stated exactly as in Section 3.1 was established for DG methods applied to the compressible Euler system, which can be regarded as a special case of the ideal MHD system with a zero magnetic field. For the compressible Euler system, one can rigorously establish a sufficient condition as in Section 3.2 for central DG methods. We will omit the proof with the focus of the current paper.

3.3. "Positivity-preserving" limiter

Given the DG solution polynomial $\mathbf{U}_h$ at time t_n, with the cell averages in the admissible set G, we will give a positivity-preserving limiter which modify $\mathbf{U}_h$ into $\tilde{\mathbf{U}}_h$ such that it will satisfy the sufficient condition given in Section 3.2 for DG methods. In fact, this limiter is almost the same as in Section 2.3 for DG methods in one dimension, as along as K and S_K are re-defined as follows: K represent a mesh element I_{ij} with any point as $\mathbf{x}$, let S_K represent the set of relevant quadrature points in $K, S_K = S_{ij}$. The numerical solution on K is denoted as $\mathbf{U}_K$.

Given the central DG solution polynomials $\mathbf{U}_h$ and $\mathbf{U}_h^D$ at time t_n, with the cell averages in the admissible set G, we will give a positivity-preserving limiter which modify $\mathbf{U}_h$ and $\mathbf{U}_h^D$ into $\tilde{\mathbf{U}}_h$ and $\tilde{\mathbf{U}}_h^D$ such that they will satisfy the sufficient condition given in Section 3.2 for central DG methods. In fact, this limiter is almost the same as in Section 2.3 for DG methods in one dimension, as long as it is applied to $\mathbf{U}_h$ and $\mathbf{U}_h^D$ separately and the notations K and S_K are re-defined as follows: On the primal mesh, let K represent a mesh element I_{ij}. Let S_K represent the set of relevant quadrature points in K, namely $S_K = \cup_{l,m=1}^{2} S_{i,j}^{l,m}$. On the dual mesh, let K represent a mesh element I_{ij}^D. Let S_K represent the set of relevant quadrature points in K, namely $S_K = S_{i,j}^{1,1} \cup S_{i,j-1}^{1,2} \cup S_{i-1,j}^{2,1} \cup S_{i-1,j-1}^{2,2}$. The numerical solution on K is denoted as $\mathbf{U}_K$.

Remark 3.1. In this paper, the positivity-preserving limiters are presented for standard DG and central DG methods. These methods use standard polynomial spaces, and the divergence-free condition on the magnetic field in (1.2) is not imposed (except for the example in Section 4.3). On the other hand, the proposed positivity preserving limiter involves an element wise convex combination of the numerical solution and its cell average. If the numerical magnetic field has zero divergence within one cell element, then after the limiter, it is still divergence-free in this element. Therefore one can apply locally divergence-free approximations [13] straightforwardly in the current framework for both DG and central DG methods without affecting the positivity-preserving property of the overall algorithm.

4. Numerical examples

In this section, numerical experiments are presented to demonstrate the performance of the proposed positivity-preserving DG and central DG methods. We start with two one-dimensional examples, namely, the high Mach shear flow and the torsional Alfvén wave pulse with periodic boundary conditions. Then our methods are tested through four two-dimensional problems including the Orzag-Tang example with the periodic boundary conditions, and the blast problem and two examples on cloud–shock interaction with outgoing boundary conditions. All the examples reported here experience negative pressure when a base scheme, namely a DG method or central DG method, is applied without the positivity-preserving limiter (PPL). With the PPL, both methods successfully remove negative pressure for all these examples. (See Remark 4.2 for other examples we tested.) In the simulations, uniform meshes are used, and the time step Δt is dynamically determined by

$$\Delta t = \frac{\alpha_0 \hat{\omega}_1}{\left(\frac{a_x}{\Delta x}\right)} \text{ (one dimension) or } \Delta t = \frac{\alpha_0 \hat{\omega}_1}{\left(\frac{a_x}{\Delta x} + \frac{a_y}{\Delta y}\right)} \text{ (two dimensions)}$$

for DG methods, and

$$\Delta t = \frac{\theta\alpha_0\hat{\omega}_1}{\left(\frac{a_x}{\Delta x}\right)} \text{ (one dimension) or } \Delta t = \frac{\theta\alpha_0\hat{\omega}_1}{\left(\frac{a_x}{\Delta x}+\frac{a_y}{\Delta y}\right)} \text{ (two dimensions)}$$

for central DG methods. Following [27] we take $\hat{\omega}_1 = 1/6$ in the second ($k = 1$) and the third order ($k = 2$) methods. Even though the analysis suggests $\alpha_0 = 1/2$, we use $\alpha_0 = 1$ for DG methods and have not observed any negative density or pressure in our experiments. Note that larger α_0 means larger time steps. For central DG methods, we still work with $\alpha_0 = 1/2$ with $\theta = 1$. The time discretization is the third order total variation diminishing (TVD) Runge–Kutta method. As mentioned in [27,23], there is a theoretical complication regarding the CFL condition for a Runge–Kutta time discretization since it is nontrivial to estimate a_x or a_y accurately for all inner stages based on the numerical solution only at time t_n. A simple technique was suggested in [27,23] by multiplying a_x and a_y with a factor when a preliminary calculation suggests negative density or pressure at time t_{n+1}. Fortunately, we haven't encountered such situation throughout the numerical experiments. Though all examples are tested with both P^1 and P^2 approximations, except for the high Mach shear flow example, we only present the P^2 results on the primal mesh.

In the presence of strong shocks, it is known that nonlinear limiters are required to control oscillations in numerical methods hence to enhance the stability of high order DG or central DG methods when simulating hyperbolic problems. We here employ the total variation bounded (TVB) minmod slope limiter, which is implemented in local characteristic fields [8,18], right before the PPL, with the associated parameter $M = 10$. Different values of M may influence the results for each individual example, and this will not be explored in this paper.

Remark 4.1. In [23], the PPL itself can stabilize high order DG schemes when simulating some very demanding examples in gaseous detonations without the TVB limiter. For DG methods, we observe that the TVB limiter must be used to stabilize the simulation, while for central DG methods, the PPL itself is sufficient for the stability of P^1 approximation yet not for the P^2 case.

Remark 4.2. We also tested widely-used MHD examples including the Brio–Wu shock tube example and the Low plasma β shock tube example [22] in one dimension, and the rotor problem [14,15] in two dimensions. No negative density or pressure is observed when the base DG and central DG methods are applied.

4.1. The high Mach shear flow

In this subsection, we consider an advected shear flow problem with high Mach number ([22]) to investigate the effectiveness and accuracy of the positivity-preserving schemes. The initial conditions are given on the domain $[0, 1]$ as

Table 4.3
Performance of DG or central DG schemes with respect to A. PP is for positivity-preserving. W means the scheme works and F means the scheme fails. NNP implies that no negative pressure is produced, while NP implies that there is negative pressure.

	$0 < A < A_s$	$A_s \leqslant A < A_p$	$A_p \leqslant A < \widetilde{A}$	$A \geqslant \widetilde{A}$
Base schemes	W/NNP	W/NP	F	F
PP schemes	W/NNP	W/NNP	W/NNP	F

Table 4.4
Values of A_p and A_s for DG schemes.

Mesh	P^1		P^2	
100	$A_s = 15$	$A_p = 20$	$A_s = 38$	$A_p = 64$
200	$A_s = 29$	$A_p = 36$	$A_s = 92$	$A_p = 150$

Table 4.5
L^2 errors for P^2 approximation of u_y for the high Mach shear flow example on $[0, 1]$ at $t = 0.02$. Error†: L^2 errors by the base methods; error††: L^2 errors by the positivity-preserving methods.

Mesh	A_s	Error†	Error††	A_s	Error†	Error††
		DG			Central DG	
100	15	1.9743E−01	1.9756E−01	15	1.5716E−01	1.5716E−01
200	29	2.7412E−01	2.7664E−01	28	2.7316E−01	2.7329E−01
400	58	3.3037E−01	3.3037E−01	61	3.3823E−01	3.3823E−01
800	115	1.0693E−01	1.0693E−01	132	2.2689E−01	2.2694E−01

$$(\rho, u_x, u_y, u_z, B_x, B_y, B_z, p) = (1, 50, A(\sin(2\pi x) + 0.15\sin(2\pi x)), 0, 0, 0, 0, 1/\gamma)$$

with periodic boundary conditions and $\gamma = 5/3$. Here, $A > 0$ is a free parameter, and one can adjust its value to demonstrate the effect of positivity-preserving limiter in the simulations. It is observed that for any given mesh, there exist two critical values for A, denoted as A_s and A_p. A_s is the smallest value for which the negative pressure appears for a base method, and no

Table 4.6
L^2 errors and orders for u_y of the high Mach shear flow example by positivity-preserving DG methods on [0, 1] at $t = 0.02$.

Mesh	L^2 error	Order	L^2 error	Order	L^2 error	Order	L^2 error	Order
	DG				Central DG			
	P^1		P^2		P^1		P^2	
200	2.60E−01	–	2.78E−01	–	2.63E−01	–	2.58E−01	–
400	6.88E−02	1.92	3.60E−02	2.95	7.96E−02	1.73	3.59E−02	2.85
800	1.03E−02	2.94	4.43E−03	3.02	1.24E−02	2.68	4.53E−03	2.99
1600	1.33E−03	2.95	5.49E−04	3.01	1.61E−03	2.94	5.48E−04	3.05

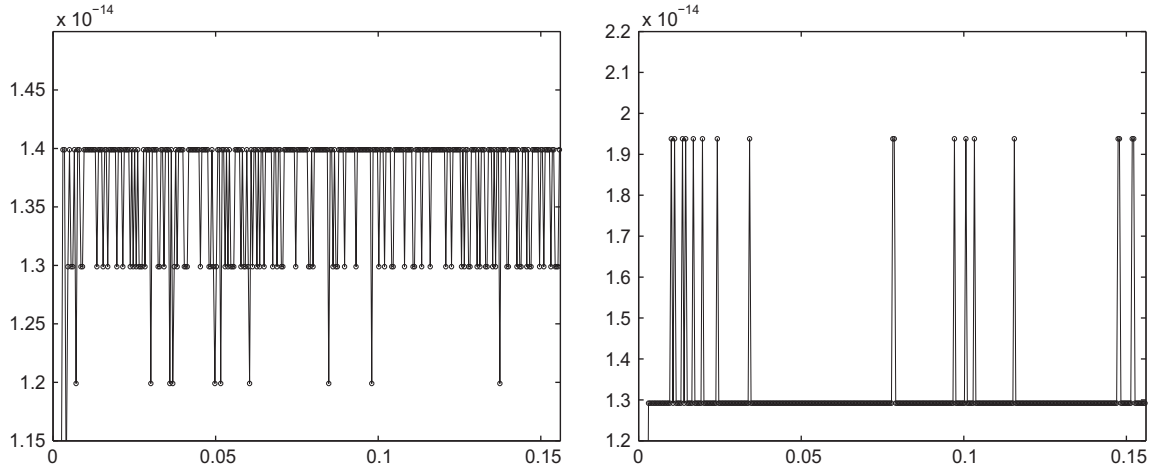

Fig. 4.2. Evolution of relative error (vertical line) of L^1 norms of density (left) and the total energy (right) versus time. Positivity-preserving DG methods.

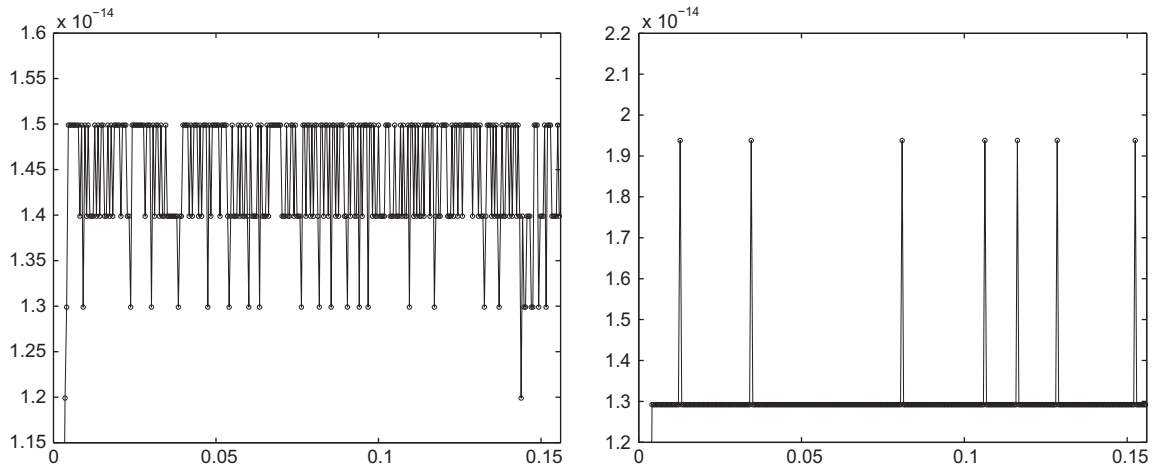

Fig. 4.3. Evolution of relative error (vertical line) of L^1 norms of density (left) and the total energy (right) versus time. Positivity-preserving central DG methods.

negative pressure is produced as $A < A_s$. A_p is the smallest value for which the base numerical scheme fails while the corresponding positivity-preserving scheme continues to work. The positivity-preserving schemes eventually break down for some $\tilde{A}$ larger than A_p. We want to point out that negative pressure does not necessarily mean the failure of a numerical method. In Table 4.3, we summarize the performance of numerical methods with respect to the values of A. Numerical tests further show that $A_p > A_s$ for both DG and central DG schemes on meshes $N = 100, 200, 400$ and 800, and this indicates that the positivity-preserving limiters stabilize the numerical simulation. As an example, we present values of A_s and A_p for DG schemes in Table 4.4 which also shows that A_s and A_p are dependent of meshsizes.

Next, we investigate the ability of positivity-preserving limiter to maintain the accuracy. We have tested various values of $A \in [A_s, A_p)$ on each mesh, and observe that the numerical errors with and without using the positivity-preserving limiter are comparable. This can be seen from Table 4.5, where L^2 errors are reported for P^2 approximations of u_y obtained by positivity-preserving DG and central DG methods as $A = A_s$.

Finally, we fix the value of A, namely, $A = 29$ for P^1 and $A = 92$ for P^2, and examine the accuracy order of the proposed methods. In Table 4.6, L^2 errors and orders are presented for u_y at $t = 0.02$, and they confirm the optimal (or better than optimal as in P^1 case) order of accuracy of the positivity-preserving DG and central DG methods. In all experiments reported for this example, the TVB limiter is not applied.

4.2. The torsional Alfvén wave pulse

Next we consider the propagation of a torsional Alfvén wave pulse ([5]) which is initialized as

$$(\rho, u_x, B_x, p) = (1, 10, 10/\sqrt{4\pi}, 0.01),$$

$$(u_y, u_z) = 10(\cos\phi, \sin\phi), \quad (B_y, B_z) = -10(\cos\phi, \sin\phi),$$

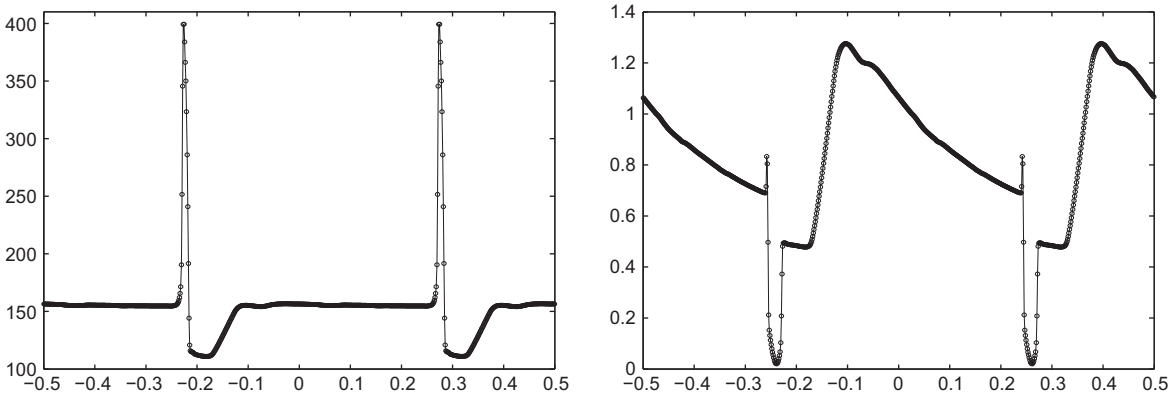

Fig. 4.4. The total energy E (left) and pressure p (right) of the torsional Alfvén wave pulse on an 800 mesh at $t = 0.156$. Positivity-preserving DG methods.

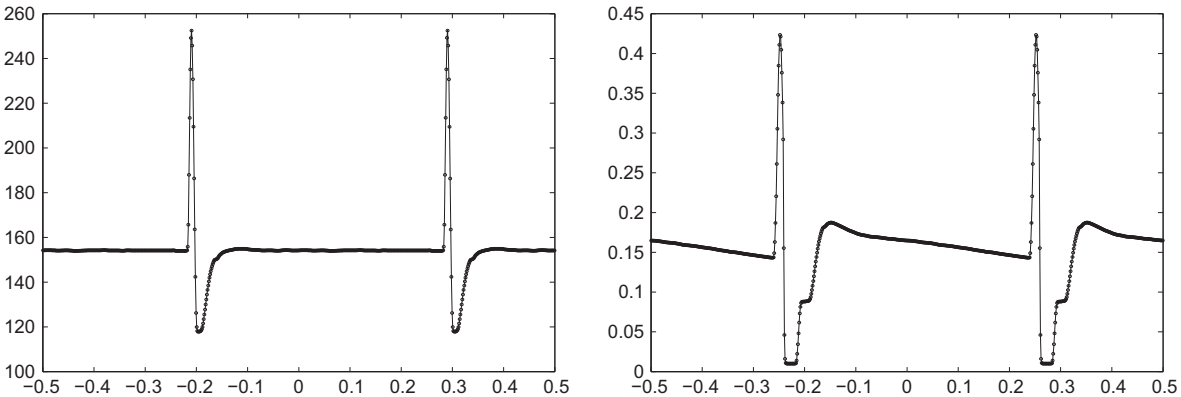

Fig. 4.5. The total energy E (left) and pressure p (right) of the torsional Alfvén wave pulse on an 800 mesh at $t = 0.156$. Positivity-preserving central DG methods.

with a pulse around the center of the computational domain $[-0.5, 0.5]$. Here $\phi = \frac{\pi}{8}(\tanh(\frac{0.25+x}{\delta}) + 1)(\tanh(\frac{0.25-x}{\delta}) + 1)$ with $\delta = 0.005$. The boundary conditions are periodic and $\gamma = 5/3$. In this example, the initial pressure is very small, which is less than ten-thousandth of the total energy. In addition to the presence of a strong torsional Alfvén wave discontinuity in the solution, it is easy for most numerical schemes to produce negative pressure.

The simulation is carried out on a uniform mesh with $N = 800$. We start with validating the L^1 stability result for density ρ and the total energy E of the positivity-preserving schemes (see Theorems 2.4 and 2.7). This in fact also corresponds to the conservation of ρ and E over the domain Ω due to the positivity of their cell average. In Figs. 4.2 and 4.3, we plot the time evolution of the relative error of $||\rho(\cdot,t)||_{L^1(\Omega)}$ and $||E(\cdot,t)||_{L^1(\Omega)}$ obtained by positivity-preserving DG and central DG methods. Both the L^1 norms of ρ and E remain constant with respect to t up to machine precision.

In Figs. 4.4 and 4.5, we further present the total energy and pressure from positivity-preserving schemes at $t = 0.156$, by then the pulse has traveled through the domain twice. Note that there are two pulses in the solution, and the successful simulation should properly preserve the shape of these features. The magnitude of the pulses in the total energy of DG solutions is larger than that of central DG methods. By taking into account the conservation, away from the pulses, the magnitude of the total energy is smaller in DG solutions. Though pressure is still much smaller than the total energy, it remains positive (in fact throughout the simulation). One can also observe the increase in pressure. In particular, in smooth region, pressure grows to about one hundredth of the total energy in DG solutions, while in central DG solutions, pressure is about one thousandth of the total energy.

In Figs. 4.6 and 4.7, we plot u_y, u_z, B_y, B_z of the positivity-preserving DG and central DG solutions, respectively. The solutions contain two discontinuities (at the location of the pulses in the total energy), and both are captured stably. In u_y and u_z, bumps can seen around one discontinuity. Similar feature is observed in [5] and it is described as shocklets and explained by the insufficiency of numerical Riemann solvers. The much smaller bump in Fig. 4.7 implies that central DG methods better capture the discontinuity for this example.

Finally we illustrate the effectiveness of the positivity-preserving limiter in eliminating negative pressure during the simulation. In Fig. 4.8, we plot the time evolution of the total number of elements with negative pressure when the base DG methods without the PPL are used. The nonzero number indicates that the PPL is activated in the simulation. For this example, the central DG methods without the PPL will blow up around $t = 0.04$.

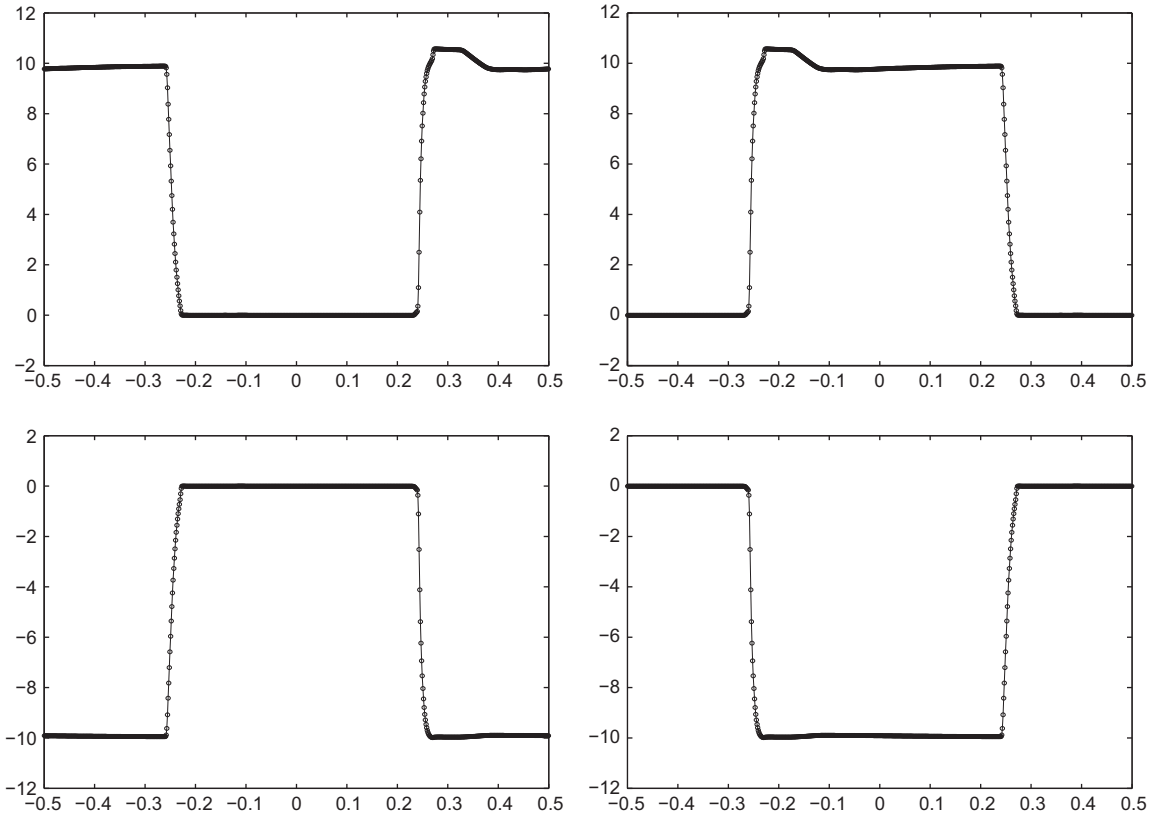

Fig. 4.6. u_y (top left), u_z (top right), B_y (bottom left), and B_z (bottom right) of the torsional Alfvén wave pulse on an 800 mesh at $t = 0.156$. Positivity-preserving DG methods.

4.3. The Orszag–Tang vortex problem

In this subsection, we consider the Orszag–Tang vortex problem which is a widely used test example in MHD simulations. The initial conditions are taken as in [13–15]

$$\rho = \gamma^2, \quad u_x = -\sin y, \quad u_y = \sin x, \quad u_z = 0,$$
$$B_x = -\sin y, \quad B_y = \sin 2x, \quad B_z = 0, \quad p = \gamma,$$

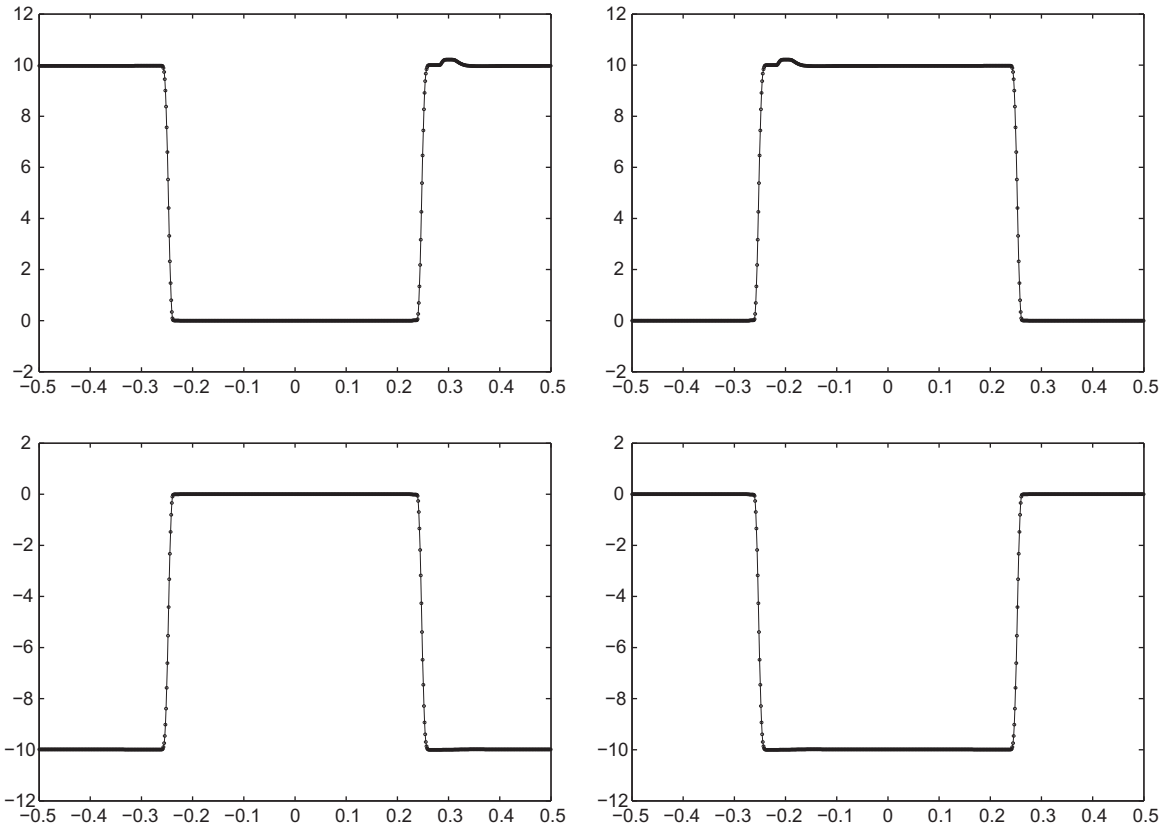

Fig. 4.7. u_y (top left), u_z (top right), B_y (bottom left), and B_z (bottom right) of the torsional Alfvén wave pulse on an 800 mesh at $t = 0.156$. Positivity-preserving central DG methods.

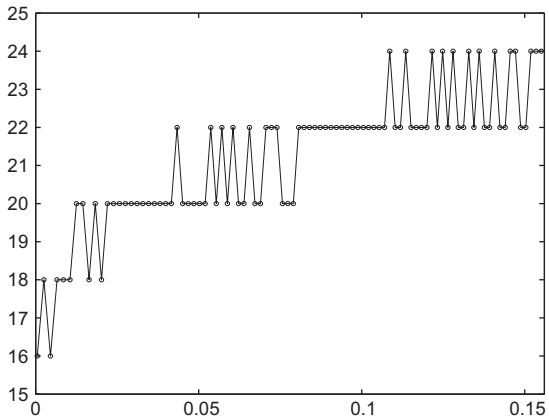

Fig. 4.8. Evolution of the total number of elements (vertical line) with negative pressure versus time. Base DG methods without the PPL.

with $\gamma = 5/3$. The computational domain is $[0, 2\pi] \times [0, 2\pi]$ with the periodic boundary conditions. The solution involves formation and interaction of multiple shocks as the nonlinear system evolves. We plot the density ρ at $t = 2$ computed by positivity-preserving DG and central DG methods on a 192×192 mesh in Fig. 4.9 which is comparable with that in [13–15].

As observed in [13], different schemes, including the same variational formulations with various solution spaces may behave differently for this example in terms of their ability to keep the simulation from breaking down. One explanation provided in [13] is the numerical divergence error. During the course of the study in [14,15] and the present work, we come

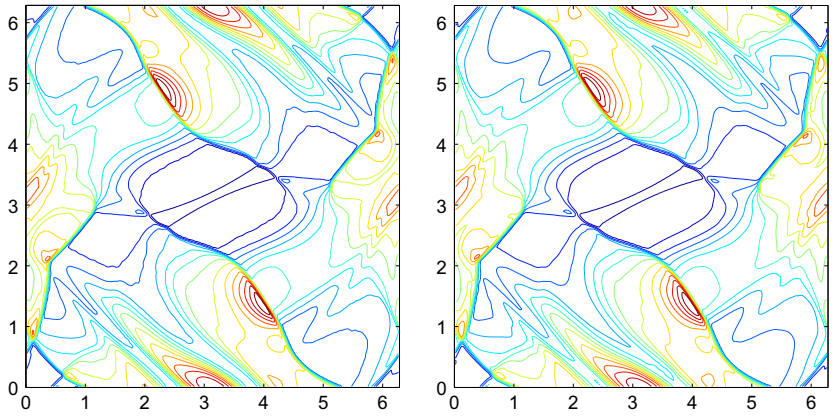

Fig. 4.9. Density ρ in Orszag–Tang vortex problem at $t = 2$ on a 192×192 mesh. Left: positivity-preserving DG methods; right: positivity-preserving central DG methods.

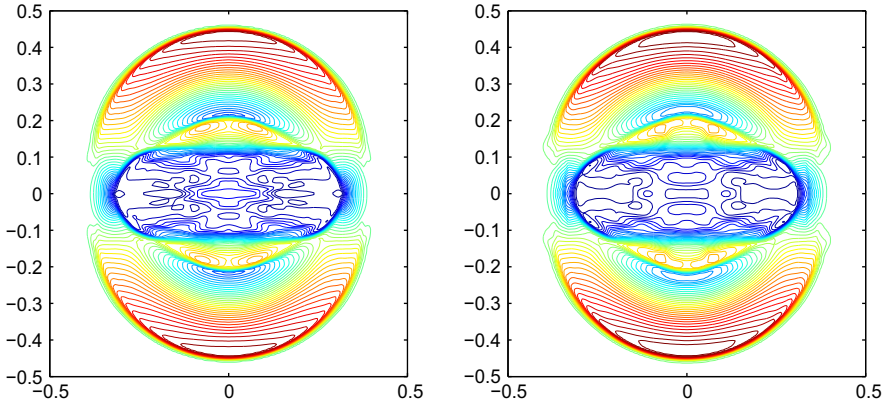

Fig. 4.10. The magnetic pressure $B_x^2 + B_y^2$ of positivity-preserving methods for the blast problem on the 200×200 mesh at $t = 0.01$. 40 equally spaced contours are used. Left: DG methods with the range of $[451.53, 1185.60]$; right: central DG methods with the range $[441.78, 1177.88]$.

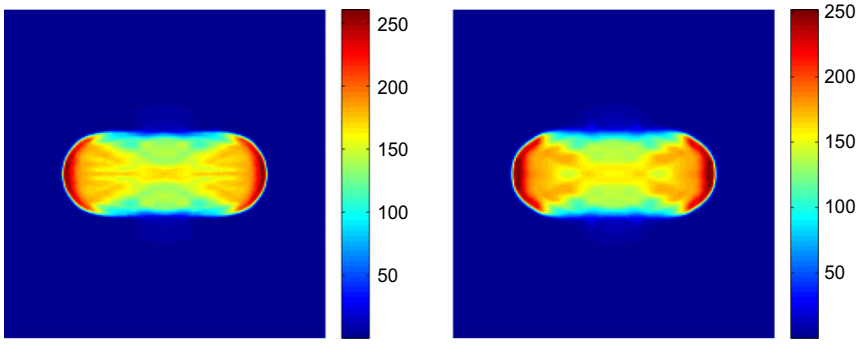

Fig. 4.11. Pressure p for the blast problem on a 200×200 mesh at $t = 0.01$. Left: positivity-preserving DG methods; right: positivity-preserving central DG methods.

to understand that negative pressure can also contribute to instability for this example. We test this example on a 192×192 mesh by using four schemes, namely, the (base) DG methods, locally divergence-free DG methods [13], positivity-preserving DG methods, and locally divergence-free positivity-preserving DG methods. Here the locally divergence-free positivity-preserving DG methods refer to the locally divergence-free DG methods in [13] to which the positivity-preserving limiter proposed in this paper is applied. With the DG methods, negative pressure starts to appear around $t = 3.2$ and the code blows up around $t = 3.6$; with the locally divergence-free DG methods, the computation breaks down around $t = 4.4$ with negative pressure being observed initially around $t = 3.7$; the negative pressure starts to appear around $t = 4.4$ and the simulation stops around $t = 4.5$ for positivity-preserving DG methods; finally, with the locally divergence-free positivity-preserving DG methods, we can simulate this example stably up to $t = 10$ (the maximum time we run, and the simulation can still go on) and there is no negative pressure in the computation. These tests show that the locally divergence-free positivity-preserving DG methods is the most robust scheme for this example, as it reduces the instability due to both the divergence error and negative pressure.

4.4. The blast problem

The blast wave problem was first introduced in [6], and the solution involves strong magnetosonic shocks. We employ the same initial condition as in [6], that is $(\rho, u_x, u_y, u_z, B_x, B_y, B_z) = (1, 0, 0, 0, 100/\sqrt{4\pi}, 0, 0)$, with the pressure given as

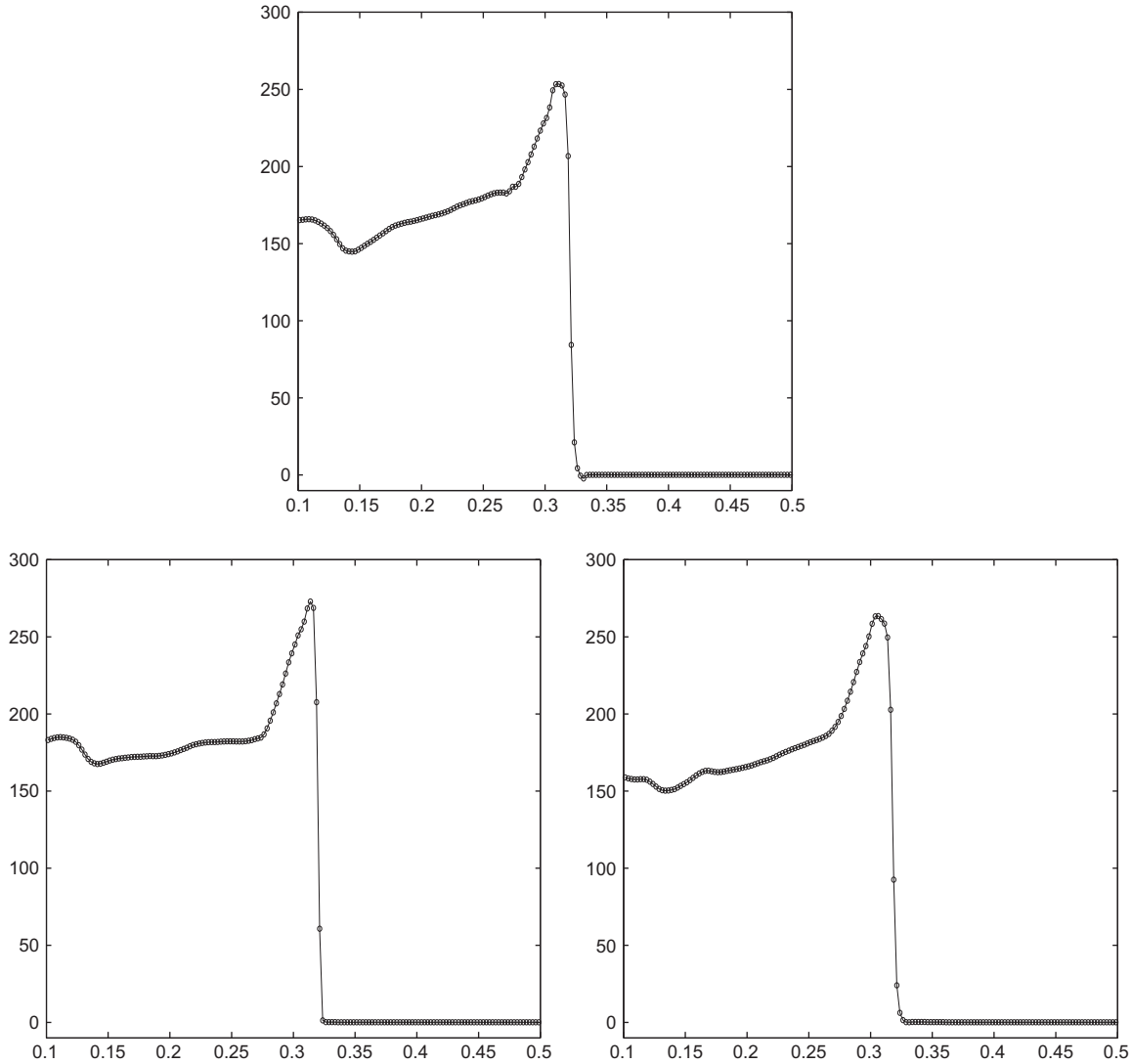

Fig. 4.12. Solution slice of pressure p for the blast problem at $t = 0.01$ with $y = 0.0$ on a 400×400 mesh. Top: base central DG method; bottom: positivity-preserving DG method (left) and positivity-preserving central DG method (right).

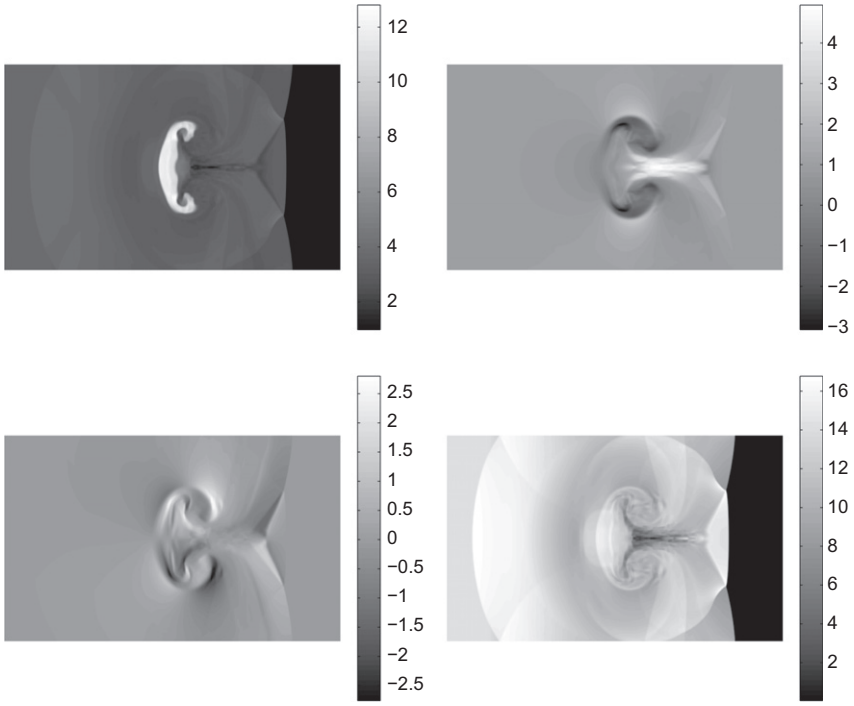

Fig. 4.13. Gray-scaled images of the numerical solution by positivity-preserving DG methods for the first cloud–shock interaction problem on a 600×300 mesh at $t = 0.3$. Top left: ρ; top right: B_x; bottom left: B_y; bottom right: p.

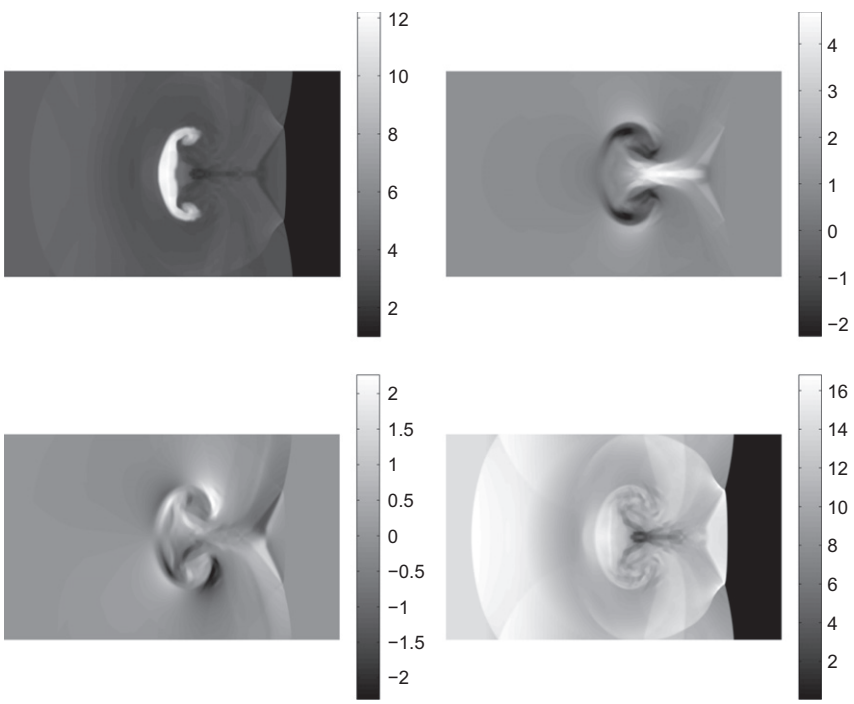

Fig. 4.14. Gray-scaled images of the numerical solution by positivity-preserving central DG methods for the first cloud–shock interaction problem on a 600×300 mesh at $t = 0.3$. Top left: ρ; top right: B_x; bottom left: B_y; bottom right: p.

$$p = \begin{cases} 1000 & \text{if } r \leqslant R, \\ 0.1 & \text{if } r > R, \end{cases}$$

where $r = \sqrt{x^2 + y^2}$ and $R = 0.1$. With this setup, the fluid in the region outside the initial pressure pulse has a very small plasma β $\left(= \frac{p}{(B_x^2 + B_y^2)/2} = 2.513E-04\right)$. The simulation is implemented in the domain $[-0.5, 0.5] \times [-0.5, 0.5]$ with the 200×200 mesh. Outgoing boundary conditions are used, and $\gamma = 1.4$. All results reported below are obtained when the TVB minmod limiter is implemented in the local characteristic fields. Such implementation of the limiter turns out to be insufficient for the stability of the exactly divergence-free central DG methods in [14,15] due to the presence of negative pressure. Instead, a componentwise TVB minmod limiter is used in [14,15] and works stably throughout the simulation.

In Fig. 4.10, we present the magnetic pressure $B_x^2 + B_y^2$ at $t = 0.01$ from the positivity-preserving DG (left) and positivity-preserving central DG methods (right). As pointed out in [6,14,15], this is a stringent problem to solve. In fact, for many commonly used numerical methods for hyperbolic conservations without being designed as positivity-preserving, negative pressure often appears near the shock front, where the jump in pressure is large and numerical oscillation can make pressure drop below zero. This is well demonstrated by the contour plots of numerical pressure by our positivity-preserving schemes in Fig. 4.11, where negative pressure is eliminated successfully in the whole domain especially around the shock front. In Fig. 4.12, we further take a closer look at the solution slices of pressure at $y = 0$ on a 400×400 mesh computed by the base

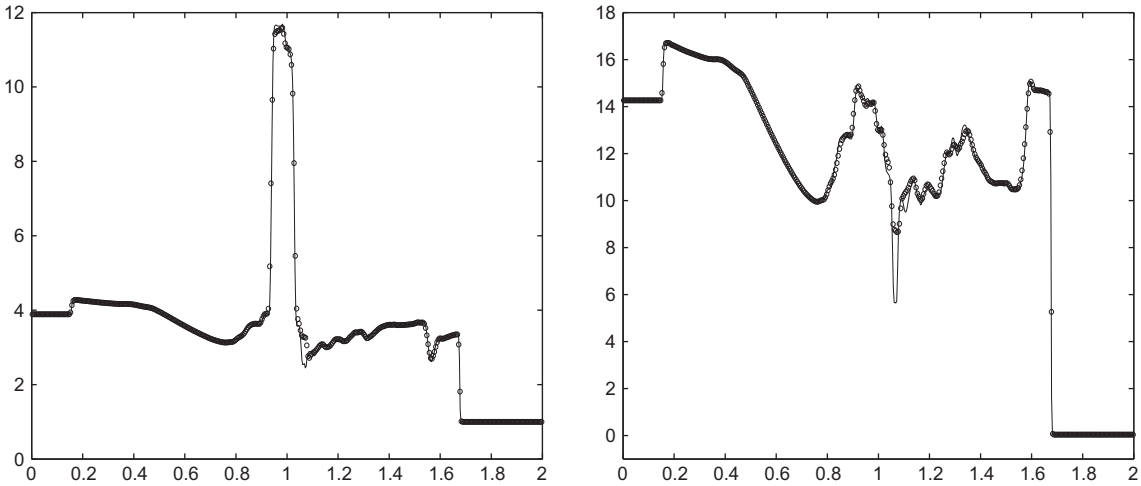

Fig. 4.15. Positivity-preserving DG approximations in the first cloud–shock interaction problem on 400×200 mesh (circle) and 600×300 (solid line) at $t = 0.3$. Left: ρ; right: p.

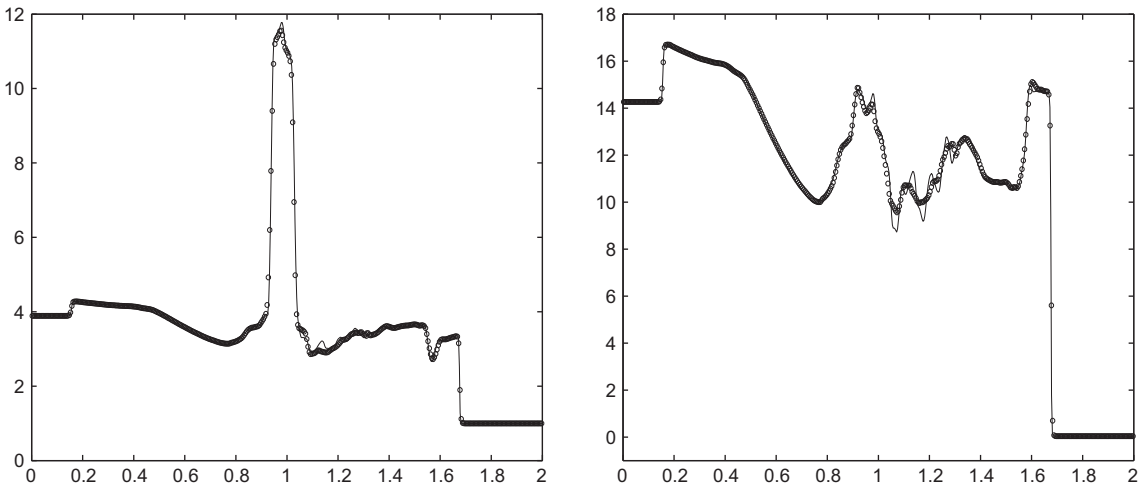

Fig. 4.16. Positivity-preserving central DG approximations in the first cloud–shock interaction problem on 400×200 mesh (circle) and 600×300 (solid line) at $t = 0.3$. Left: ρ; right: p.

central DG method, the positivity-preserving DG method and the positivity-preserving central DG method. It is clear that negative pressure appears near the shock front ($x = 0.325$) for the base central DG method, yet it is removed with the

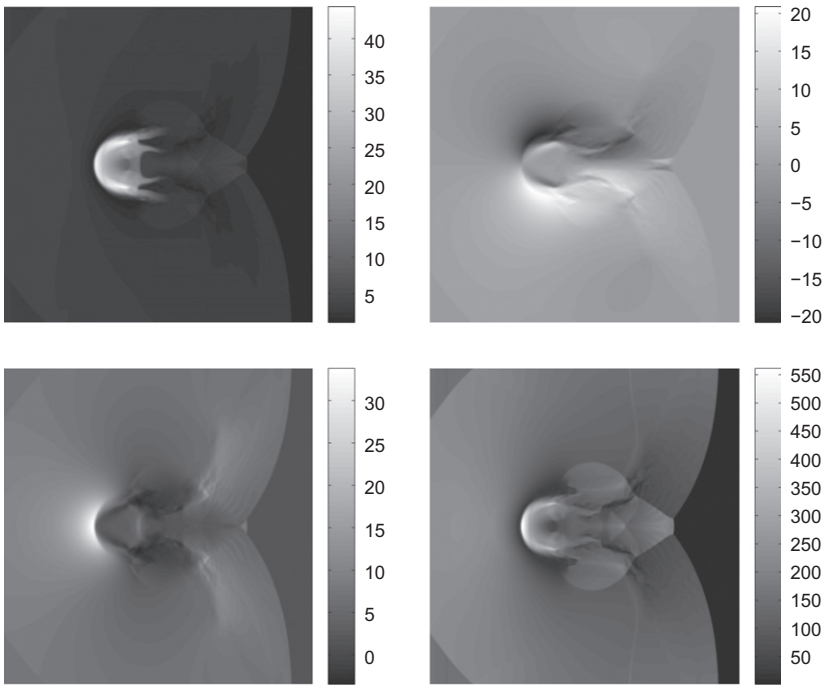

Fig. 4.17. Gray-scaled images for P^2 DG approximations of the second cloud–shock interaction problem on the 400×400 mesh at $t = 0.06$. Top left: ρ; top right: B_x; bottom left: B_y; bottom right: p.

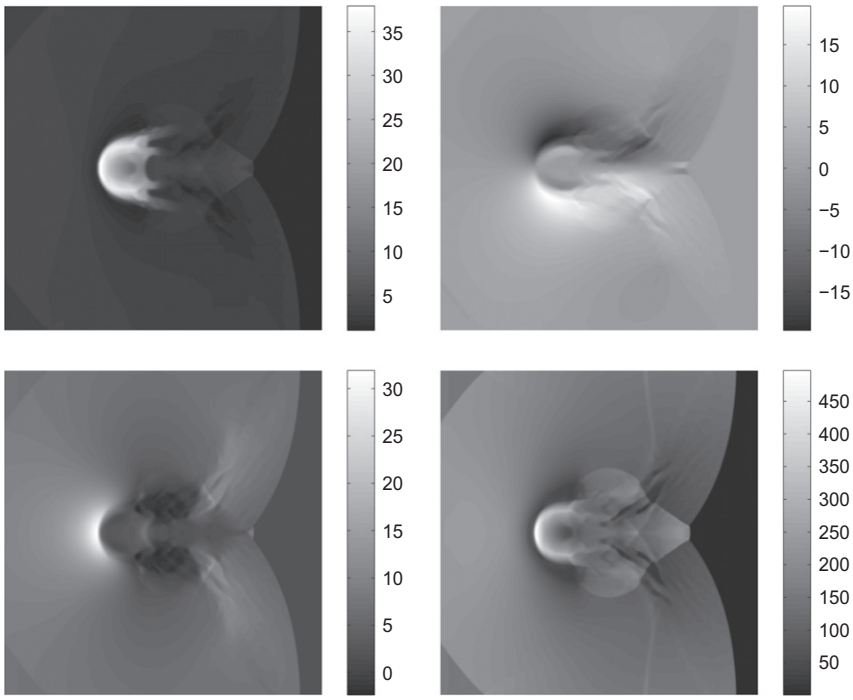

Fig. 4.18. Gray-scaled images for P^2 central DG approximations of the second cloud–shock interaction problem on the 400×400 mesh at $t = 0.06$. Top left: ρ; top right: B_x; bottom left: B_y; bottom right: p.

use of the positivity-preserving limiter. In addition, the numerical pressure by positivity-preserving DG method is sharper around the discontinuity.

4.5. The cloud–shock interaction

In this section, we consider two examples of cloud–shock interaction which involve strong MHD shocks interacting with a dense cloud.

For the first cloud–shock interaction example [14], we define three sets of data for $(\rho, u_x, u_y, u_z, B_x, B_y, B_z, p)$ as

$$\mathbf{U}_1 = (3.88968, 0, 0, -0.05234, 1, 0, 3.9353, 14.2614),$$

$$\mathbf{U}_2 = (1, -3.3156, 0, 0, 1, 0, 1, 0.04), \quad \mathbf{U}_3 = (5, -3.3156, 0, 0, 1, 0, 1, 0.04).$$

The computational domain $[0,2] \times [0,1]$ is divided into three regions: the post-shock region $\Omega_1 = \{(x,y) : 0 \leqslant x \leqslant 1.2, 0 \leqslant y \leqslant 1\}$, the pre-shock region $\Omega_2 = \{(x,y) : 1.2 < x \leqslant 2, 0 \leqslant y \leqslant 1, \sqrt{(x-1.4)^2 + (y-0.5)^2} \geqslant 0.18\}$, and the cloud region $\Omega_3 = \{(x,y) : \sqrt{(x-1.4)^2 + (y-0.5)^2} < 0.18\}$. The solutions in Ω_1, Ω_2 and Ω_3 are initialized as $\mathbf{U}_1, \mathbf{U}_2$, and $\mathbf{U}_3$, respectively. Outgoing boundary conditions are used, and $\gamma = 5/3$. Note that the cloud taking up the region Ω_3 is five times denser than

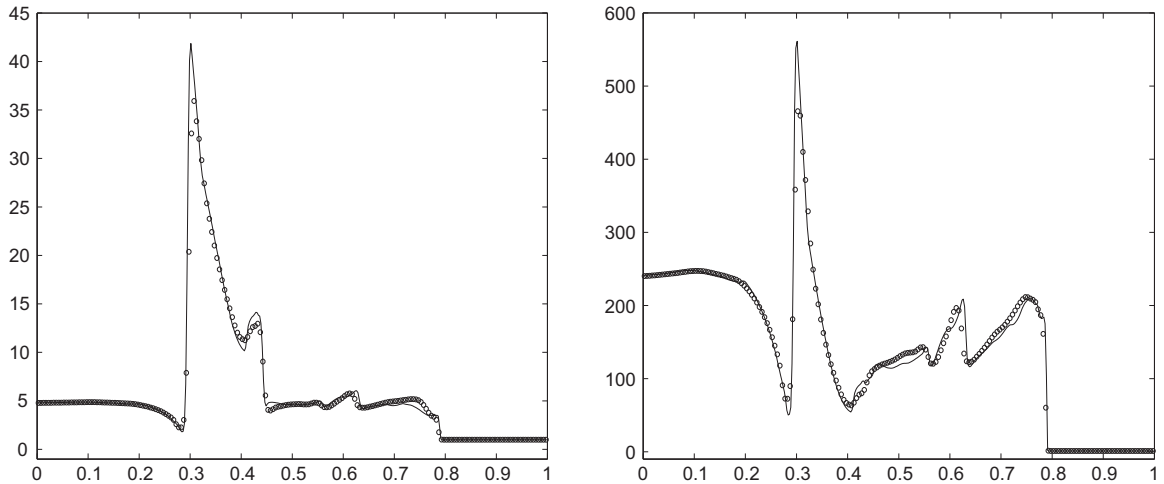

Fig. 4.19. The P^2 DG approximations in the second cloud–shock interaction problem on the 200×200 mesh (circle) and the 400×400 (solid line) at $t = 0.06$. Left: ρ; right: p.

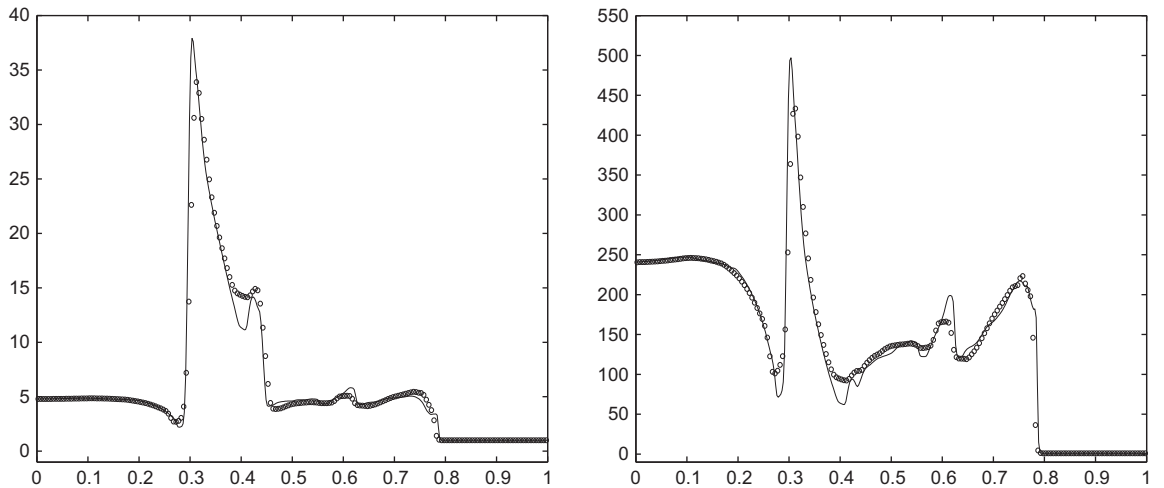

Fig. 4.20. The P^2 central DG approximations in the second cloud–shock interaction problem on the 200×200 mesh (circle) and the 400×400 (solid line) at $t = 0.06$. Left: ρ; right: p.

its surrounding, and the pressure in the post-shock region is about hundreds times of that in the pre-shock region. When $t \in (0, 0.35)$, negative pressure is observed in the simulation of the base DG and central DG methods. In fact, negative pressure also appears in the globally divergence-free central DG methods [14,15] and the locally divergence-free DG methods [13]. (After $t = 0.35$, the shock front propagates out of the computational domain, there is no longer negative pressure.)

With the positivity-preserving limiters, there is no negative pressure observed in DG and central DG simulations during $t \in (0, 0.35)$. Fig. 4.13 (positivity-preserving DG methods) and Fig. 4.14 (positivity-preserving central DG methods) also show the gray-scale images of the solution on a 600×300 mesh. The results are for density ρ, the magnetic field component B_x and B_y, and the pressure p at $t = 0.3$, when quite much feature has developed in the solution. To further illustrate the convergence and positivity-preserving property of the methods, we present in Fig. 4.15 (positivity-preserving DG methods) and Fig. 4.16 (positivity-preserving central DG methods) the solution slices of density ρ and pressure p at $y = 0.6$ on 400×200 and 600×300 meshes. The convergence of the proposed methods is observed, with the pressure perfectly preserved to be positive around the shock front.

For the second cloud–shock interaction example [9], we define three sets of data for $(\rho, u_x, u_y, u_z, B_x, B_y, B_z, p)$ as

$$\mathbf{U}_1 = (3.86859, 0, 0, 0, 0, 0, 7.73718, -7.73718, 167.345),$$

$$\mathbf{U}_2 = (1, -11.2536, 0, 0, 0, 2, 2, 1), \quad \mathbf{U}_3 = (10, -112.536, 0, 0, 0, 2, 2, 1).$$

The computational domain $[0, 1] \times [0, 1]$ is divided into three regions: the post-shock region $\Omega_1 = \{(x, y) : 0 \leqslant x \leqslant 0.6, 0 \leqslant y \leqslant 1\}$, the pre-shock region $\Omega_2 = \{(x, y) : 0.6 < x \leqslant 1, 0 \leqslant y \leqslant 1, \sqrt{(x-0.8)^2 + (y-0.5)^2} \geqslant 0.15\}$, and the cloud region $\Omega_3 = \{(x, y) : \sqrt{(x-0.8)^2 + (y-0.5)^2} < 0.15\}$. The solutions in Ω_1, Ω_2 and Ω_3 are initialized as $\mathbf{U}_1, \mathbf{U}_2$, and $\mathbf{U}_3$ respectively. Outgoing boundary conditions are used, and $\gamma = 5/3$. Note that the cloud taking up the region Ω_3 is ten times denser than its surrounding. Although the pressure in the post-shock region is also about hundreds times of that in the pre-shock region, the initial discontinuity in pressure is much stronger compared with the first cloud–shock problem. In fact, our globally divergence-free schemes in [14,15] fail to simulate this example due to the negative pressure. With positivity-preserving limiters, our proposed methods solve this problem stably.

Fig. 4.17 (positivity-preserving DG methods) and Fig. 4.18 (positivity-preserving central DG methods) show the gray-scale images on a 400×400 mesh for density ρ, the magnetic field component B_x and B_y, and the pressure p at $t = 0.06$. No negative pressure is observed. We also present in Fig. 4.19 (positivity-preserving DG methods) and Fig. 4.20 (positivity-preserving central DG methods) the solution slices of density ρ and pressure p at $y = 0.5$ computed on 200×200 and 400×400 meshes. The convergence of the proposed methods is observed, while the pressure stays positive around the shock front.

5. Concluding remarks

In this paper, high order positivity-preserving DG and central DG schemes are proposed for ideal MHD equations in one and two dimensions on Cartesian meshes. These methods can be extended to general meshes, or to MHD systems with different equations of states. Within the DG setting, one can further take advantage of the advances in the design of various one- or multi-dimensional Riemann solvers for MHD equations [19,11,4], to obtain other first order (hopefully provable) positivity preserving schemes in one or multiple dimensions, which can serve as building blocks for positivity preserving methods with high order accuracy. In the framework of central DG methods, one can follow the sequence of work by Zhang and Shu to develop maximum-principle-satisfying limiters for scalar conservation laws [26] and the positivity-preserving schemes for compressible Euler equations [27]. Some tools which can be used to analyze these methods can be seen in Section 2.2.

Appendix A. To examine positivity-preserving property of the first order Lax–Friedrichs DG method in the presence of discontinuous B_x

As in Section 2.1.1, we here carry out some numerical experiments to examine whether the first order DG method with the Lax–Friedrichs flux in (2.7)–(2.9) is positivity-preserving *when B_x is discontinuous*. We start with three vectors $\mathbf{U}_{i-1}^n, \mathbf{U}_i^n$ and $\mathbf{U}_{i+1}^n$ which take random values. In particular u_x, u_y, u_z, B_y and B_z are from $U(-\gamma_1, \gamma_1), \rho$ is from $U(0, \gamma_2), p$ is from $U(0, \gamma_3)$, and B_x is from $U(-\gamma_4, \gamma_4)$. Here $U(\gamma_\star, \gamma_{\star\star})$ is the uniform distribution on $(\gamma_\star, \gamma_{\star\star})$. We also vary the CFL number λa_x within $[1/2, 1]$. For each set of parameters $\gamma_i, i = 1, \ldots 4$ and λa_x, we conduct 10^5 random experiments, compute $\mathbf{U}_i^{n+1}$ from (2.7)–(2.9), and count the total number of occurrence of negative pressure, namely when $p(\mathbf{U}_i^{n+1}) < 0$. The results in Table A.7 are collected when $\lambda a_x = 1/2$, and they show that the first order Lax–Friedrichs DG method (2.7)–(2.9) is positivity-preserving under the CFL condition 2.10 with $\lambda a_x = (\leqslant)\alpha_0 = 1/2$. Numerical tests further indicate that this positivity-preserving property holds for a larger CFL condition such as $\alpha_0 = 3/5$ yet not for very large α_0, see Table A.8. Note that in our experiments B_x can have very large jump which may not necessarily be encountered in reasonable numerical simulations for the MHD system.

References

[1] D.S. Balsara, Self-adjusting, positivity preserving high order schemes for hydrodynamics and magnetohydrodynamics, Journal of Computational Physics 231 (2012) 7504–7517.
[2] D.S. Balsara, T. Rumpf, M. Dumbser, C.-D. Munz, Efficient, high accuracy ADER–WENO schemes for hydrodynamics and divergence-free magnetohydrodynamics, Journal of Computational Physics 228 (2009) 2480–2516.
[3] D.S. Balsara, Divergence-free reconstruction of magnetic fields and WENO schemes for magnetohydrodynamics, Journal of Computational Physics 228 (2009) 5040–5056.
[4] D.S. Balsara, A two-dimensional HLLC Riemann solver for conservation laws: application to Euler and magnetohydrodynamic flows, Journal of Computational Physics 231 (2012) 7476–7503.
[5] D.S. Balsara, D. Spicer, Maintaining pressure positivity in magnetohydrodynamic simulations, Journal of Computational Physics 148 (1999) 111–148.
[6] D.S. Balsara, D.S. Spicer, A staggered mesh algorithm using high order Godunov fluxes to ensure solenoidal magnetic fields in magnetohydrodynamic simulations, Journal of Computational Physics 149 (1999) 270–292.
[7] J.U. Brackbill, D.C. Barnes, The effect of nonzero $\nabla \cdot \mathbf{B}$ on the numerical solution of the magnetohydrodynamic equations, Journal of Computational Physics 35 (1980) 426–430.
[8] B. Cockburn, C.-W. Shu, The Runge–Kutta discontinuous Galerkin method for conservation laws V: Multidimensional systems, Journal of Computational Physics 141 (1998) 199–224.
[9] W. Dai, P.R. Woodward, A simple finite difference scheme for multidimensional magnetohydrodynamic equations, Journal of Computational Physics 142 (1998) 331–369.
[10] C.R. Evans, J.F. Hawley, Simulation of magnetohydrodynamic flows: a constrained transport method, Astrophysical Journal 332 (1988) 659–677.
[11] K.F. Gurski, An HLLC-type approximate Riemann solver for ideal magnetohydrodynamics, SIAM Journal on Scientific Computing 25 (2004) 2165–2187.
[12] P. Janhunen, A positive conservative method for magnetohydrodynamics based on HLL and Roe methods, Journal of Computational Physics 160 (2000) 649–661.
[13] F. Li, C.-W. Shu, Locally divergence-free discontinuous Galerkin methods for MHD equations, Journal of Scientific Computing 22 (2005) 413–442.
[14] F. Li, L. Xu, S. Yakovlev, Central discontinuous Galerkin methods for ideal MHD equations with the exactly divergence-free magnetic field, Journal of Computational Physics 230 (2011) 4828–4847.
[15] F. Li, L. Xu, Arbitrary order exactly divergence-free central discontinuous Galerkin methods for ideal MHD equations, Journal of Computational Physics 231 (2012) 2655–2675.
[16] Y. Liu, C.-W. Shu, E. Tadmor, M. Zhang, Central discontinuous Galerkin methods on overlapping cells with a nonoscillatory hierarchical reconstruction, SIAM Journal on Numerical Analysis 45 (2007) 2442–2467.
[17] B. Perthame, C.-W. Shu, On positivity preserving finite volume schemes for Euler equations, Numerische Mathematik 73 (1996) 119–130.
[18] K.G. Powell, An Approximate Riemann Solver for Magnetohydrodynamics (That Works in More Than One Dimension), ICASE Report No. 94-24, Langley, VA, 1994.
[19] P.L. Roe, D.S. Balsara, Notes on the eigensystem of magnetohydrodynamics, SIAM Journal on Applied Mathematics 56 (1996) 57–67.
[20] J. Smoller, Shock Waves and Reaction–diffusion Equations, Grundlehren der mathematischen Wissenschaften 258, Springer Verlag, 1994.
[21] G. Tóth, The $\nabla \cdot \mathbf{B} = 0$ constraint in shock-capturing magnetohydrodynamics codes, Journal of Computational Physics 161 (2000) 605–652.
[22] K. Waagan, A positive MUSCL–Hancock scheme for ideal magnetohydrodynamics, Journal of Computational Physics 228 (2009) 8609–8626.
[23] C. Wang, X. Zhang, C.-W. Shu, J. Ning, Robust high order discontinuous Galerkin schemes for two-dimensional gaseous detonations, Journal of Computational Physics 231 (2012) 653–665.
[24] Z. Xu, Y. Liu, C.-W. Shu, Hierarchical reconstruction for discontinuous Galerkin methods on unstructured grids with a WENO type linear reconstruction and partial neighboring cells, Journal of Computational Physics 228 (2009) 2194–2212.
[25] S. Yakovlev, L. Xu, F. Li, Locally divergence-free central discontinuous Galerkin methods for ideal MHD equations, Journal of Computational Sciences, http://dx.doi.org/10.1016/j.jocs.2012.05.002.
[26] X. Zhang, C.-W. Shu, On maximum-principle-satisfying high order schemes for scalar conservation laws, Journal of Computational Physics 229 (2010) 3091–3120.
[27] X. Zhang, C.-W. Shu, On positivity preserving high order discontinuous Galerkin schemes for compressible Euler equations on rectangular meshes, Journal of Computational Physics 229 (2010) 8918–8934.